Subduction history of the Tethyan region derived from seismic tomography and tectonic reconstructions

E. Hafkenscheid,[1,2] M. J. R. Wortel,[1] and W. Spakman[1]

Received 20 April 2005; revised 16 February 2006; accepted 29 March 2006; published 8 August 2006.

[1] In the mantle underneath the Tethyan suture zone, large volumes of positive velocity anomalies have been imaged by seismic tomography and interpreted as the present-day signature of subducted Tethyan lithosphere. We investigate the Mesozoic-Cenozoic subduction history of the region by integrating independent information from mantle tomography and tectonic reconstructions. Three different subduction scenarios for the Tethyan oceanic lithosphere, representative for the available tectonic reconstructions, are used to predict the present thermally anomalous volumes associated with the lithospheric surface subducted since the late Mesozoic. Next, these predicted thermal volumes and their expected positions are compared to the relevant anomalous volumes derived from seismic tomographic images. In this analysis we include, among others, the possible effects of ridge subduction and slab detachment after the Cenozoic continental collisions, absolute plate motion, and slab thickening in the mantle. Our preferred subduction model comprises the opening of large back-arc oceanic basins within the Eurasian margin. The model points to slab thickening by a factor of 3 in the mantle, in which case the estimated volumes allow for active oceanic spreading ($\sim$1–2.5 cm/yr) in the Tethyan lithosphere during convergence. Our results further indicate the occurrence of early Oligocene slab detachment underneath the northern Zagros suture zone, followed by both westward and eastward propagation of the slab tear and diachronous Eocene to Miocene slab detachment below the eastern to western Himalayas. Free sinking rates of the detached material of $\sim$2 cm/yr in the lower mantle provide the best fit between the tomographic mantle structure and our Tethyan subduction model.

Citation: Hafkenscheid, E., M. J. R. Wortel, and W. Spakman (2006), Subduction history of the Tethyan region derived from seismic tomography and tectonic reconstructions, *J. Geophys. Res.*, *111*, B08401, doi:10.1029/2005JB003791.

1. Introduction

[2] Seismic tomography has revealed the presence of several great belts of positive velocity anomalies in the Earth's mantle [e.g., *van der Hilst et al.*, 1997; *Bijwaard et al.*, 1998] that have been interpreted as the present-day signature of subducted lithospheric material [e.g., *Richards and Engebretson*, 1992; *Wen and Anderson*, 1995; *Bunge et al.*, 1998; *Lithgow-Bertelloni and Richards*, 1998]. Among these, the seismic anomalous volume underneath the Tethyan suture zone, marked today by the Alpine-Zagros-Himalayan mountain belt, is one of the largest and most prominent ones. It is generally accepted that this volume stems from the subduction of the large Tethyan oceanic basins and the subsequent collision of the Eurasian continent with the Arabian and Indian subcontinents.

[3] More specific ideas concerning the Tethys Oceans subduction and the relative motion of the continents involved have been formulated in terms of plate tectonic reconstructions [e.g., *Dercourt et al.*, 1993; *Şengör and Natal'in*, 1996; *Norton*, 1999; *Stampfli and Borel*, 2004]. These reconstructions are based on many integrated sets of geological and geophysical near-surface data, and thus contain invaluable information on the timing of the regional kinematics. The currently available data sets, however, have not yet allowed the definition of one single geodynamic scenario for the Tethyan evolution. Seismic tomography has provided entirely new information on the present mantle structure, which has not played a role in the formulation of the tectonic reconstructions. Therefore combining seismic tomography with available reconstructions constitutes an optimal way to further explore the plate boundary evolution and subduction process in the Tethyan realm. Our approach here is to investigate which of the existing tectonic reconstructions, and their implicitly proposed subduction scenarios, provides the best agreement with the 3D mantle structure inferred from seismic tomography.

[4] Comparisons of tomographic models with thermal modeling results have led to a better understanding of the geodynamic evolution (back to $\sim$80 Ma) of active subduction zones all over the world [e.g., *De Jonge et al.*, 1994; *Deal et al.*, 1999; *Bunge and Grand*, 2000; *Daniel et al.*,

[1]Vening Meinesz Research School of Geodynamics, Faculty of Geosciences, Utrecht University, Utrecht, Netherlands.
[2]Now at Shell International Exploration & Production, Rijswijk, Netherlands.

0148-0227/06/2005JB003791$09.00

2001; *Schmid et al.*, 2002]. In the Tethyan region, however, connecting the long-time (~200 Myr) history of subduction to the tomographic mantle structure has been hampered owing to the large-scale deformation caused by the final continental collisions, the almost complete disappearance of the Tethyan oceanic lithosphere, and the large amount of subduction. As a result, comparisons between plate tectonic reconstructions and seismic tomography models for the Tethyan region have so far been largely qualitative of character [e.g., *Van der Voo et al.*, 1999; *Replumaz et al.*, 2004].

[5] To arrive at a more quantitative reconstruction of the Mesozoic-Cenozoic subduction of the Tethys Oceans, we will here develop a method to integrate plate tectonic reconstructions, mantle tomography, and elements of subduction dynamics. As schematically illustrated in Figure 1, we therefore (1) calculate the surface of subducted lithosphere "Su" from a tectonic reconstruction, (2) define the initial thermal volumes "Vi" of the subducted lithosphere calculated in step 1, (3) predict the present thermal volumes "Vp" of the slabs from the volumes defined in step 2, (4) estimate the size of the anomalous volumes in seismic tomography "Vt" that may be related to subducted lithosphere, and (5) compare the anomalous tomographic volumes "Vt" estimated in step 4 with the present thermal volumes "Vp" predicted in step 3.

[6] The effects of subduction-related processes, for which the kinematic boundary conditions are implicitly given by the tectonic reconstructions, are incorporated in the first three steps. We will also take into account the further possible behavior of the slabs in the mantle, as well as absolute plate motion, in the final comparison with the tomography models. As different reconstructions will generally lead to different predictions of the sizes and locations of the present thermal volumes, a systematic comparison of these to the volumes and positions of the tomographic anomalies will enable us to evaluate the quality of the reconstructions and subduction scenarios involved.

2. Mesozoic-Cenozoic Evolution of the Tethyan Region

2.1. Tethyan Evolution and Its Tectonic Reconstructions

[7] In Mesozoic times, the Tethys Oceans separated the Africa-Arabian and Indian continents from Eurasia. With the opening of the Atlantic Ocean (~180 Ma), the continents started to converge and the oceans gradually began closing. The eventual continental collisions initiated the formation of the impressive Alpine-Zagros-Himalayan mountain chain in the Cenozoic, from ~50 Ma onward. The subduction of the Tethys Oceans has thus been dominated by the movements of the largest continents. However, the process has been complicated by the continuous rifting of various intermediate fragments, back-arc spreading and intraoceanic subduction.

[8] We will here investigate the subduction history of the Tethyan region on the basis of the tectonic reconstructions of *Dercourt et al.* [1993], *Şengör and Natal'in* [1996], *Norton* [1999], and *Stampfli and Borel* [2002, 2004]. The first three reconstructions can be viewed upon as classical continental drift models, while those of *Stampfli and Borel* [2002, 2004] are further constrained by dynamic plate boundaries. As an example, the Late Cretaceous reconstruction of *Stampfli and Borel* [2004] is shown in Figure 2. Although the reconstructions agree on the first-order continent-continent motions in the Tethyan region, no overall consensus has been achieved on the more detailed evolution of the plate boundaries and subduction zones.

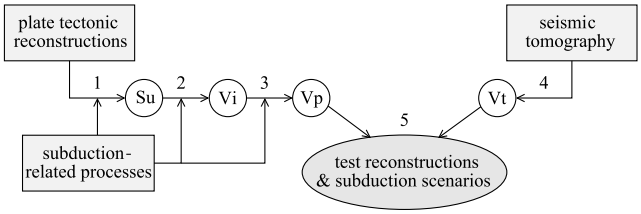

Figure 1. Schematic representation of our approach: Comparison of (1) reconstruction-derived surface (Su), (2) initial thermal volumes (Vi), and (3) present thermal volumes (Vp) of the subducted lithosphere versus (4) the tomographic volumes (Vt) that may be related to these remnants in order (5) to test the underlying tectonic reconstructions c.q. subduction scenarios. Subduction-related processes are incorporated in the first three steps.

2.2. Surface Tectonics Versus Subduction

[9] Both the large-scale similarities and second-order differences between the proposed surface processes in the Tethyan region may help us to better understand and constrain the subduction processes in the underlying mantle. We here address those aspects of the tectonic evolution that may have had major implications for the specific subdivision, relative distribution and geometry of the lithosphere subducted. The uncertainties in the tectonic reconstructions, and thus the actual errors in the predicted volumes derived from these later, are difficult to assess. To arrive at robust conclusions, we will therefore focus on the large-scale, first-order features in our analyses.

2.2.1. Subduction of Oceanic Ridges and Back-Arc Basins

[10] For the Mesozoic history of subduction, we analyze the effect of subduction of the Neo-Tethyan lithosphere and spreading ridge, and the possible role of the subduction of large oceanic back-arc basins. From the tectonic reconstructions of *Dercourt et al.* [1993], *Şengör and Natal'in* [1996], *Norton* [1999], and *Stampfli and Borel* [2002, 2004] we derive three typical subduction scenarios for the Tethyan region. These scenarios obey the main kinematic boundary conditions for the subduction process implicitly proposed by the different reconstructions. Motions of intermediate fragments and local plate boundary deformation, e.g., the recent trench migration within the Aegean area, are not taken into account for this large-scale analysis.

[11] The subduction scenarios especially differ in the subduction of the spreading ridges and separate oceanic basins. As the morphology of the subducted material may have been affected by these processes, and the downgoing slab may end up as separate or apparently interrupted thermal volumes, we expect to be able to evaluate the

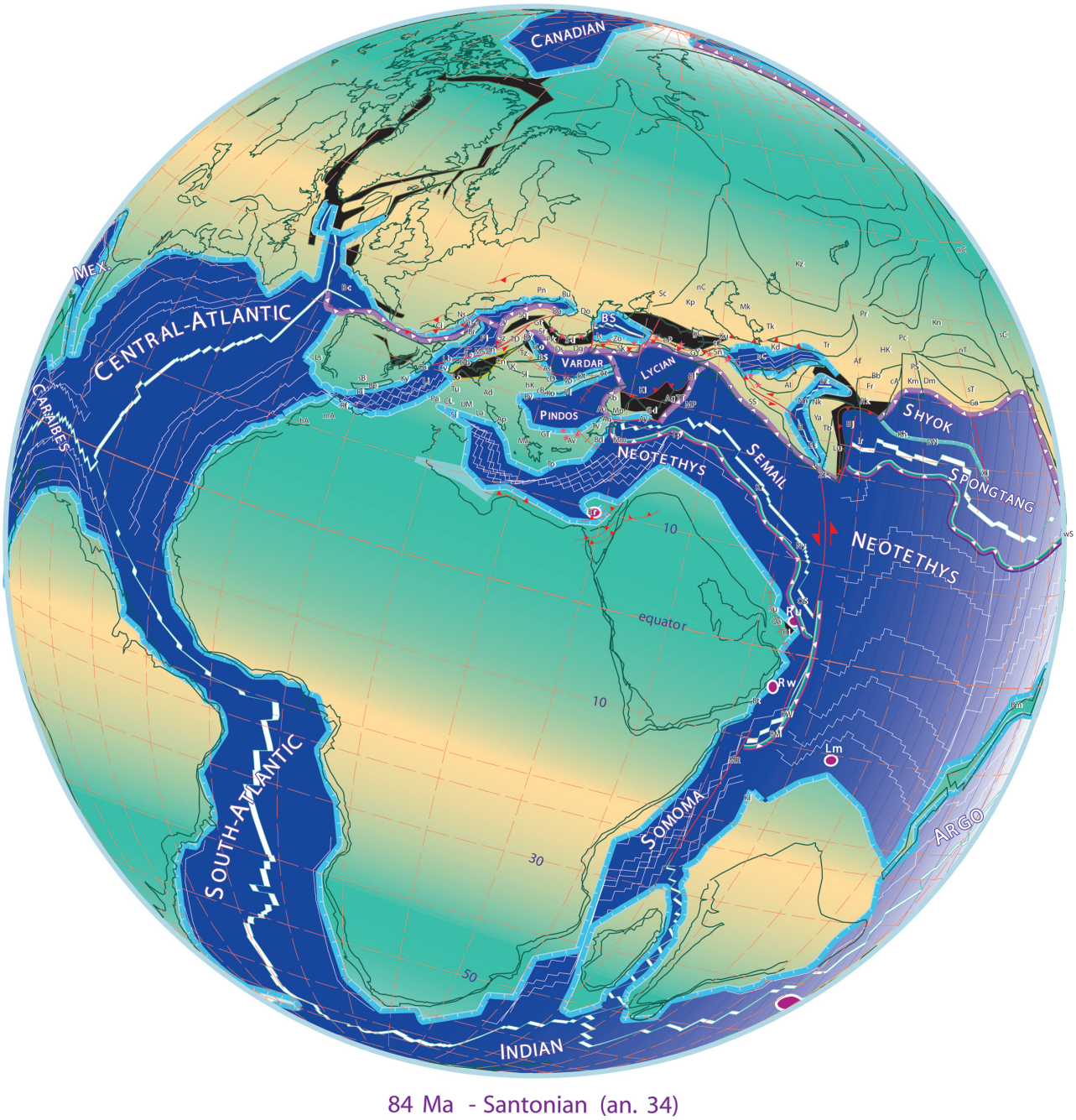

Figure 2. Late Cretaceous reconstruction of *Stampfli and Borel* [2004]. Note the presence of the Semail and Spongtang oceanic back-arc basins between the Neo-Tethys and Eurasian continental margin. Published with kind permission of the author and Springer Science and Business Media.

qualities of the scenarios on this point. We emphasize that we test the reconstructions underlying the three subduction scenarios as they are, i.e., without an a priori judgment of their merits and shortcomings.

[12] The first subduction scenario (Figure 3, top) is the most straightforward one, proposed for the subduction of the Neo-Tethys by *Norton* [1999] and (for the Indian region only) by *Şengör and Natal'in* [1996]. In this scenario, all relative motion between the converging African/Arabian/Indian and Eurasian continents, as well as the subduction of the Neo-Tethyan spreading ridge around 80 Ma, is accommodated along one single trench system at the Eurasian margin.

[13] The second subduction scenario (Figure 3, middle) is often proposed for the Arabian region [e.g., *Dercourt et al.*, 1993; *Şengör and Natal'in*, 1996] to explain the ~80 Ma emplacement time of the Oman ophiolites on the Arabian continental margin. In this scenario, Neo-Tethyan crust obducted onto the Arabian continental margin by thrusting or during a short period of intraoceanic subduction. The amount of lithosphere subducted at this location is proposed to have been small. As in scenario I, basically all lithosphere

is subducted underneath the Eurasian margin. We note that this subduction scenario is not proposed for the Indian region.

[14] The third subduction scenario (Figure 3, bottom) is based on the work by *Stampfli and Borel* [2002, 2004] for both the Arabian and Indian region. This scenario assumes an early (~140–120 Ma) subduction of the Neo-Tethyan ridge to have triggered the opening of two distinct back-arc basins within the Eurasian margin: The Semail Ocean in the Middle East and the Spongtang Ocean in the Indian region (see Figure 2). Because spreading within these back-arc oceans occurs at the direct expense of the Neo-Tethys, this adds to the amount of subduction as calculated from the converging continents alone. In the Arabian region, the Neo-Tethys disappears completely just before the obduction of Semail ophiolites onto the Arabian margin around ~80 Ma, through intraoceanic subduction. For simplicity, we assume that at that moment the Semail Ocean starts to subduct northward underneath Eurasia instead. In the Indian region, the moment of Neo-Tethyan disappearance and Spongtang obduction is around 65 Ma, at which moment we also assume the initiation of subduction underneath Eurasia.

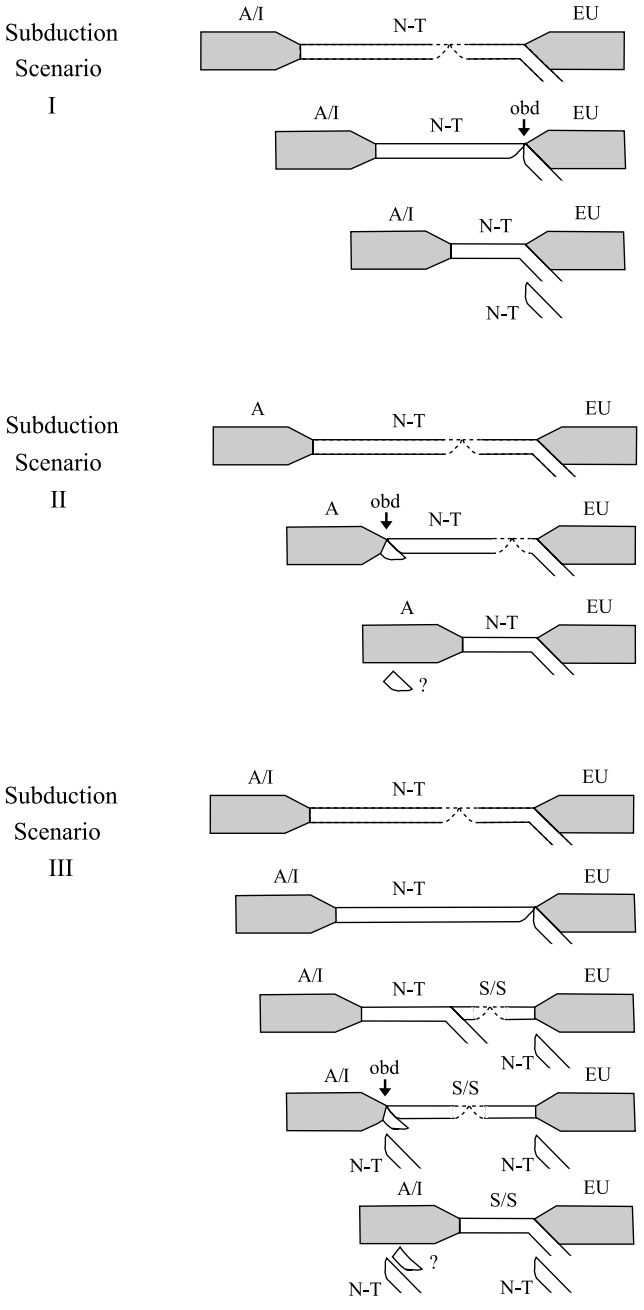

Figure 3. Three subduction scenarios for the Tethys Oceans. In subduction scenario I, all Neo-Tethyan subduction is accommodated along one single trench system at the Eurasian margin. In subduction scenario II (only for the Arabian region), Neo-Tethyan ophiolites are emplaced onto the Arabian margin by thrusting or during a short period of intraoceanic subduction, but basically all Neo-Tethyan lithosphere is subducted along the same Eurasian trench system. In subduction scenario III, Neo-Tethyan ridge subduction underneath Eurasia is followed by the opening of a Semail/Spongtang back-arc basin. After this oceanic basin has completely overridden the Neo-Tethys and ophiolites are obducted onto the Arabian/Indian margin, its lithosphere is subducted below Eurasia. The different subduction scenarios will lead to different predictions of the present volumes and positions of the subducted oceanic domains. A, Arabian continent; I, Indian continent; EU, Eurasian continent; N-T, Neo-Tethys Ocean; S/S, Semail/Spongtang Ocean; and obd, ridge obduction.

2.2.2. Cenozoic Continental Collisions

[15] The most recent history of subduction is marked by continental collision processes. There is general agreement that the first continental parts of Greater India collided with the Eurasian continent in the early Eocene. Time estimates for the onset of collision of Arabia with Eurasia range from late Eocene to early Miocene times. In this study, we will start with the approximate accretion times from *Norton* [1999] of 48 Ma and 22 Ma, respectively. In addition, an earlier onset of the Arabia-Eurasia collision, e.g., proposed by *Dercourt et al.* [1993], will be considered. If subsequent slab detachment (break off) occurred, the present-day depth and location of the detached material must be in accordance with the timing of break off. Also the volumes, both of the slab broken off and the lithosphere still attached to the surface, may help us on this point.

2.3. Slab Behavior in the Mantle

[16] As illustrated in Figure 1, the possible behavior of the slabs in the mantle will be incorporated in the comparison of the models. This component is needed to make the link between the reconstructed surface evolution and the mantle tomography. Many of the geodynamic processes involved have been well investigated in numerous observational, laboratory and numerical modeling studies.

2.3.1. Subducted Oceanic Ridges and Back-Arc Basins

[17] The oceanic spreading centers between converging and colliding continents, either active or not, eventually subduct underneath the overriding continental margins. When an active or fossil ridge subducts, either asthenospheric material fills the space between the diverging plates such that a slab window is formed, or the major thermal differences between the two subducting plates rapidly

disappear because of thermal diffusion. Also when a distinct oceanic basin has subducted, the slab material may be imaged as a separate volume in tomographic models.

2.3.2. Slab Detachment After Continental Collisions

[18] Continent-continent collisions can cause slabs to break off and sink into the mantle, as shown by modeling studies [e.g., *Davies and von Blanckenburg*, 1995; *Wong A Ton and Wortel*, 1997; *Van de Zedde and Wortel*, 2001] and observational evidence [e.g., *Carminati et al.*, 1998; *Wortel and Spakman*, 2000]. On the basis of the accretion times and convergence velocities derived from the tectonic reconstructions, we will investigate whether the Tethyan continental collisions have also caused the subducted slabs to break off and, if so, at what time.

2.3.3. Slab Thickening

[19] Laboratory and numerical modeling studies, as well as observational studies [e.g., *Lay*, 1994], have shown that slabs can significantly deform during their descent into the mantle. Slabs subducting slowly at small angles may already have thickened to twice their original width by the time they reach the base of the transition zone [e.g., *Gaherty and Hager*, 1994; *Becker et al.*, 1999], while fast and steeply subducting slabs can fold and thicken by at least a factor of 2–3 when they enter the more viscous lower mantle [e.g., *Gaherty and Hager*, 1994; *Christensen*, 1996]. We should thus expect the Tethyan subducted slab material to have thickened as well, particularly in the lower mantle. Only smaller slabs in the upper mantle may have remained largely unthickened.

2.3.4. Slab Rollback

[20] Trench migration is an effective mechanism for generating shallow dipping slabs [e.g., *Griffiths et al.*, 1995; *Guillou-Frottier et al.*, 1995; *Christensen*, 1996; *Olbertz et al.*, 1997], and flattened slab structures below trenchward migrating, still active subduction zones have been globally imaged by seismic tomography, e.g., underneath the Izu-Bonin, Sunda, and Tonga island arcs [e.g., *van der Hilst*, 1995; *Bijwaard et al.*, 1998; *Kárason and van der Hilst*, 2000; *Hall and Spakman*, 2002]. Also direct observational evidence for present-day slab rollback has been published, e.g., for the Aegean region by *McClusky et al.* [2000]. Because subduction scenario III proposes the Neo-Tethyan lithosphere to have gradually disappeared underneath the spreading back-arc basins, the slab may have significantly flattened accordingly in this case.

2.3.5. Sinking Rates

[21] In the upper mantle, estimates of the vertical sinking rates of slabs are comparable to plate convergence rates. When slabs enter the lower mantle, the large viscosity contrast with the upper mantle causes the sinking rates to be reduced significantly. Estimates of slab sinking rates through the lower mantle range from 1 to 3 cm/yr [e.g., *Lithgow-Bertelloni and Richards*, 1998; *Han and Gurnis*, 1999], with the faster rates typically associated with sinking in regions with abundant subduction in the same area [*Steinberger*, 2000].

2.4. Absolute Motion

[22] Whereas the division and relative distribution of the subducted lithosphere will depend on the assumed subduction scenario, the actual geographical location of the slab material is a function of the absolute motion of the plates since the time of subduction. Comparing the present positions of the various tomographic anomalies to the past locations of the relevant trench systems may therefore help us to further evaluate the subduction scenarios.

[23] To account for the present uncertainties in defining absolute plate motion [e.g., *Tarduno and Gee*, 1995; *Norton*, 2000; *Torsvik et al.*, 2002; *O'Neill et al.*, 2003], we will here consider three different reference frames: One in which the Eurasian craton is held fixed (EU), a fixed hot spot reference frame constructed from *Duncan and Richards* [1991] for the past 30 Ma and from *Müller et al.* [1993] prior to that time (HS), and the hot spot reference frame of *O'Neill et al.* [2003] based on the motion of hot spots in the Indian Ocean (MHS). Although the relative positions of the larger continental blocks are quite well known, their absolute locations can differ as much as 10° for the time and reference frames considered here.

3. Tomographic Mantle Structure Interpreted as Subducted Tethyan Lithosphere

3.1. Interpretation of Seismic Anomalies in Terms of Temperature

[24] To assess the anomalous volumes in the deep mantle thought to represent the slab remnants of the Tethys Oceans, we use the tomographic *P* wave velocity model of *Bijwaard et al.* [1998]. Representative vertical and horizontal cross sections through this model are shown in Figures 4 and 5. The model has a global and whole mantle coverage yielding sufficient detail because cell sizes have been adapted to sampling density. In general, continental and tectonically active regions like the Tethyan area are relatively well sampled, and well resolved. Here the resolution is approximately 65–100 km laterally and 35–65 km vertically in the upper mantle. In the lower mantle, the lateral resolution is about 150–300 km and the vertical resolution 100–200 km at best [see *Bijwaard et al.*, 1998; *Van der Voo et al.*, 1999]. The exact resolution of the tomographic model, and thus the actual errors in the tomographic volumes derived from these later, are unknown. We will necessarily take the tomographic model as it is, and will account for the uncertainties as much as possible. Also here we will focus on the large-scale features in the model.

[25] Most seismological studies suggest that seismic velocity anomalies in the mantle, in particular those associated with subducted and relatively cold material, are primarily caused by temperature variations [e.g., *Forte et al.*, 1994; *Ranalli*, 1996; *Röhm et al.*, 2000; *Trampert et al.*, 2001; *Goes and van der Lee*, 2002]. To interpret the subduction-related velocity anomalies in terms of thermal perturbations, we here use the depth-dependent temperature derivatives of seismic *P* wave velocities. Currently available compilations and estimates of the anharmonic temperature derivatives from *Karato* [1993], *De Jonge et al.* [1994], *Trampert et al.* [2001] and *Cammarano et al.* [2003] are shown in Figure 6. From these values, we construct a minimum and maximum profile down to 2600 km depth to define the boundary of each tomographic anomaly. The relevant anomalies underneath the Tethyan region can all be found well above this depth (see Figures 4 and 5). Anomalies in the top 230 km of the model will not be analyzed because the seismic velocities in this depth interval are

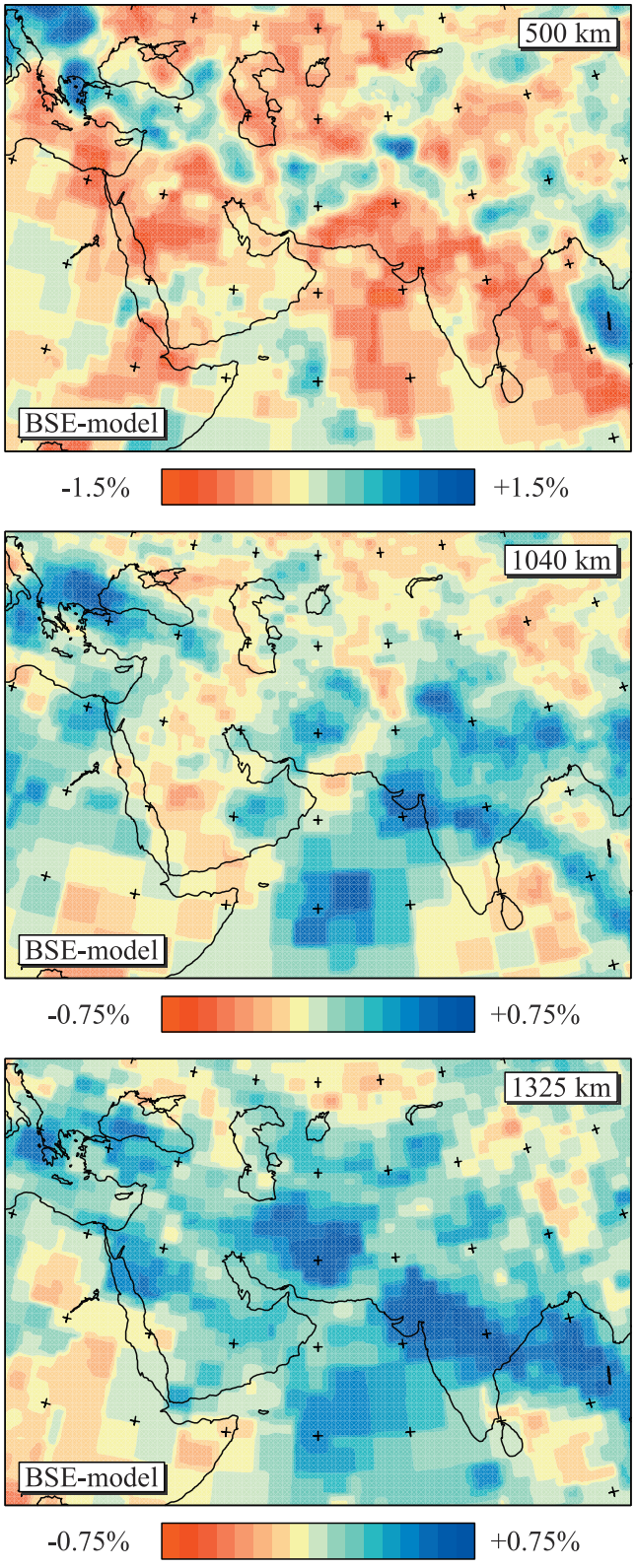

Figure 4. Horizontal sections through the tomographic model of *Bijwaard et al.* [1998] at 500, 1040, and 1325 km depth.

likely to be highly influenced by compositional heterogeneities, strong attenuation and marked elastic anisotropy.

3.2. Quantification of Anomalous Volumes

[26] The volumes of the Tethyan anomalies are determined from a series of cross sections through the tomographic model (Figure 7, top). The sections are separated by 0.5° each, and crossed halfway by a great circle that follows the general orientation of the lower mantle anomalies (cf. Figure 4). Within each vertical cross section, we determine those areas that reveal velocity anomalies higher than the cutoff values for ΔV_p that follow the minimum and maximum profiles of Figure 6 and correspond to thermal perturbations of −100°C. As the amplitudes of the inverted velocity anomalies are probably damped by 20–30% [*Bijwaard and Spakman*, 2000], these thermal perturbations are likely to be underestimated by a similar percentage. To account for the uncertainty in the seismic anomalies [*Bijwaard et al.*, 1998], values of ΔV_p smaller than 0.2% will be ignored. Assuming that the anomalous areas are representative for the small segment surrounding each cross section, we directly calculate the volumes for these section segments by multiplying all areas with the appropriate dimensions. We note that the use of the minimum profile of Figure 6 will provide us with an upper limit, and the maximum profile with a lower limit, of the tomographic volumes.

3.3. Identification of Separate Tomographic Volumes

[27] The section segment volumes, calculated above, that are thought to belong to the same anomalous volumes within the model are grouped together. To identify a single anomalous body, the resolution of the tomographic model is taken into account. Because of its spatial variation, the actual resolution for each tomographic image needs to be investigated separately. The various anomalous bodies that are recognized throughout the Tethyan region are shown in Figure 8, in which the contour line of each body is a projection of its maximum horizontal extension in the given depth interval. We note that some of these bodies might belong to the same single volumes, but this cannot be decided on the basis of the tomography model alone. We leave this as a possibility to be decided on later in this study. The tomographic volumes were referred to as "Vt" in Figure 1 (step 4). The anomalies beneath Myanmar and former Yugoslavia that can be seen in Figure 4 are situated outside our region of interest. Furthermore, the deep positions of the anomalies underneath central Asia, far north of the Cenozoic Zagros suture zone, suggest that these are related to an earlier phase of subduction (see also *Van der Voo et al.* [1999] and section 6). For an extensive discussion on the identification of the Tethyan anomalies, we refer to *Hafkenscheid* [2004].

4. Thermal Signature of Subducted Tethyan Lithosphere Predicted From Reconstructions

4.1. Calculation of Subducted Plate Surface From Tectonic Reconstructions

[28] To assess the total amount of convergence since 200 Ma, we calculate the displacements of the Africa-Arabian and Indian continents with respect to Eurasia from

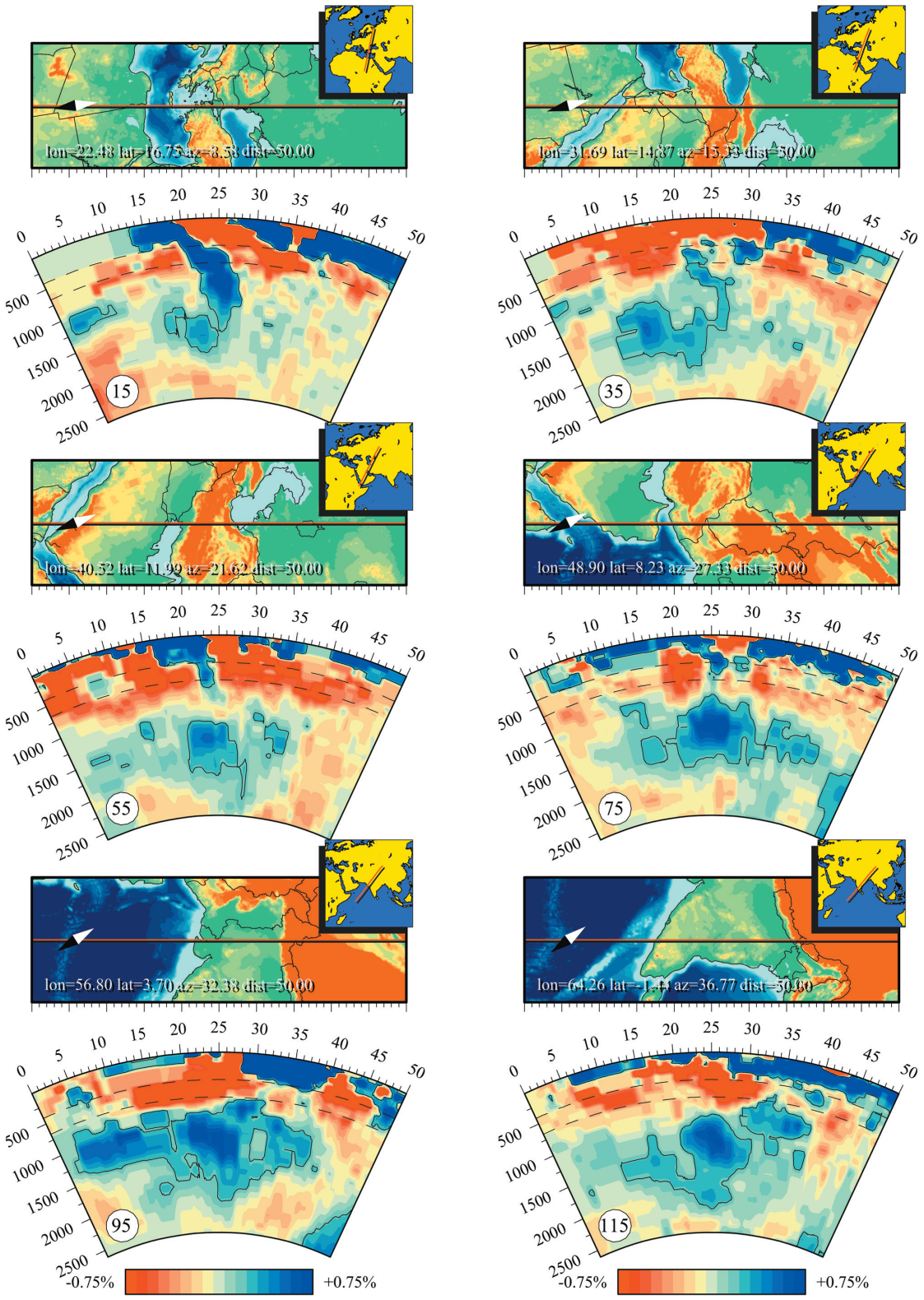

Figure 5. Vertical sections through the tomographic model of *Bijwaard et al.* [1998], as indicated in Figure 8, down to 2600 km depth. In each section the 0.2% contour lines, indicating the approximate maximum volumes calculated, are shown as well.

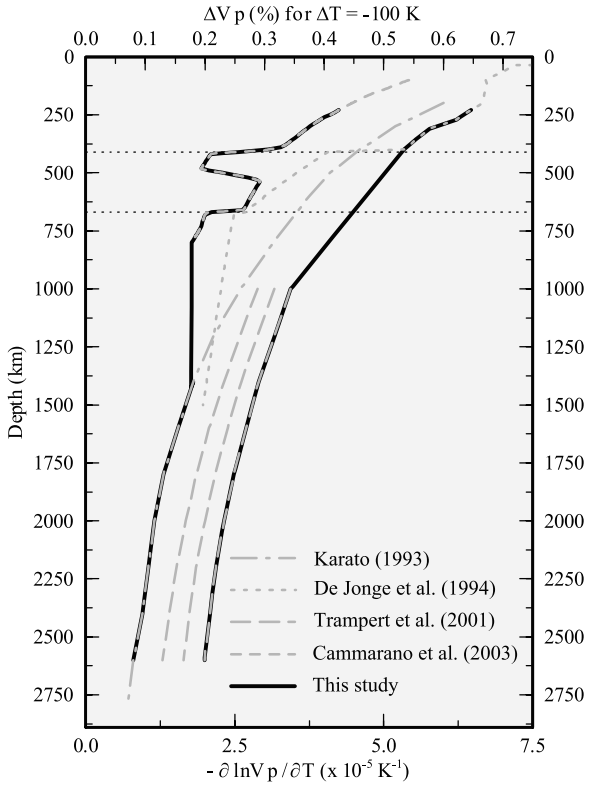

Figure 6. Distribution of anharmonic temperature derivatives of seismic *P* wave velocities. Grey dashed lines indicate values based on estimates from *Karato* [1993], *De Jonge et al.* [1994], *Trampert et al.* [2001], and *Cammarano et al.* [2003]. Black lines indicate minimum and maximum profiles used in this study. Also indicated (top *X* axis) are the associated seismic velocity anomalies ΔVp (%) expected for a thermal perturbation ΔT of −100 K.

the digitized reconstruction of *Norton* [1999]. Because the reconstructions of *Dercourt et al.* [1993], *Şengör and Natal'in* [1996], and *Stampfli and Borel* [2002, 2004] propose similar relative motions for these continents, we assume the continent-continent displacements to be the same for all three subduction scenarios defined in Figure 3. The subduction of the large back-arc oceanic basins proposed in subduction scenario III will be addressed separately in section 6.

[29] Because the present-day trenches and suture zones in the Tethyan region are intensely deformed by the latest stages of continental collision, we will use a roughly NW-SE trending line at which to evaluate the rate and amount of convergence at. For this "trench" line, we take the same great circle that was used to define the cross sections through the tomographic model (see Figure 7, bottom). The exact location of the trench system will not significantly affect the outcome of our calculations. Keeping the trench system fixed to the Eurasian plate through time, the calculations on convergence are performed at the same points along the great circle that were crossed by the sections used to analyze the tomographic model. We split up the Aegean and Arabian regions at section 31, presently the approximate boundary between the African and Arabian plates. Section 87, roughly aligned with the boundary between the Arabian and Indian plates, is chosen to split up the Arabian and Indian regions.

[30] In Figure 9 it can be seen that the calculated amount of convergence increases from west to east, as the total poles of rotation are positioned just west of the Tethyan area. The plate surface subducted per region is now approximated by multiplying the estimated convergence at each point by the 0.5° width of the trench segment that separates the point from its adjoined points. This surface of subducted Tethyan lithosphere was denoted "Su" in Figure 1 (step 1). The calculated amount of subducted material can be considered as a minimum value because

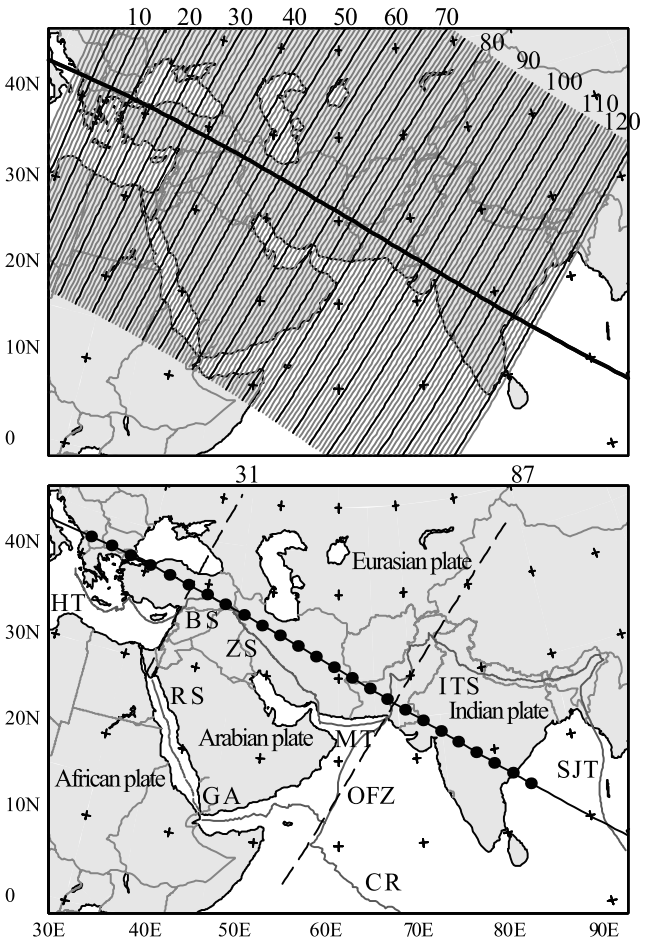

Figure 7. (top) Cross sections used to analyze the anomalies in the tomographic model underneath the Tethyan region, with every fifth section highlighted here. The sections are crossed halfway by a great circle that is roughly aligned with the deep positive velocity anomalies in the tomographic model. (bottom) "Trench" points at which the total amount of convergence is calculated, with every fifth point plotted here. The great circle taken as the trench line is the same as the one used in Figure 7 (top). Present-day trenches and suture zones are HT, Hellenic Trench; BS, Bitlis Suture; ZS, Zagros Suture; MT, Makran Trench; ITS, Indus-Tsangpo Suture; and SJT, Sunda-Java Trench. Main active features are rifts in the RS, Red Sea, and GA, Gulf of Aden, as well as the OFZ, Owen Fracture Zone, and CR, Carlsberg Ridge. The area is divided into an Aegean region (points 1–31), Arabian region (points 31–87), and Indian region (points 87–126).

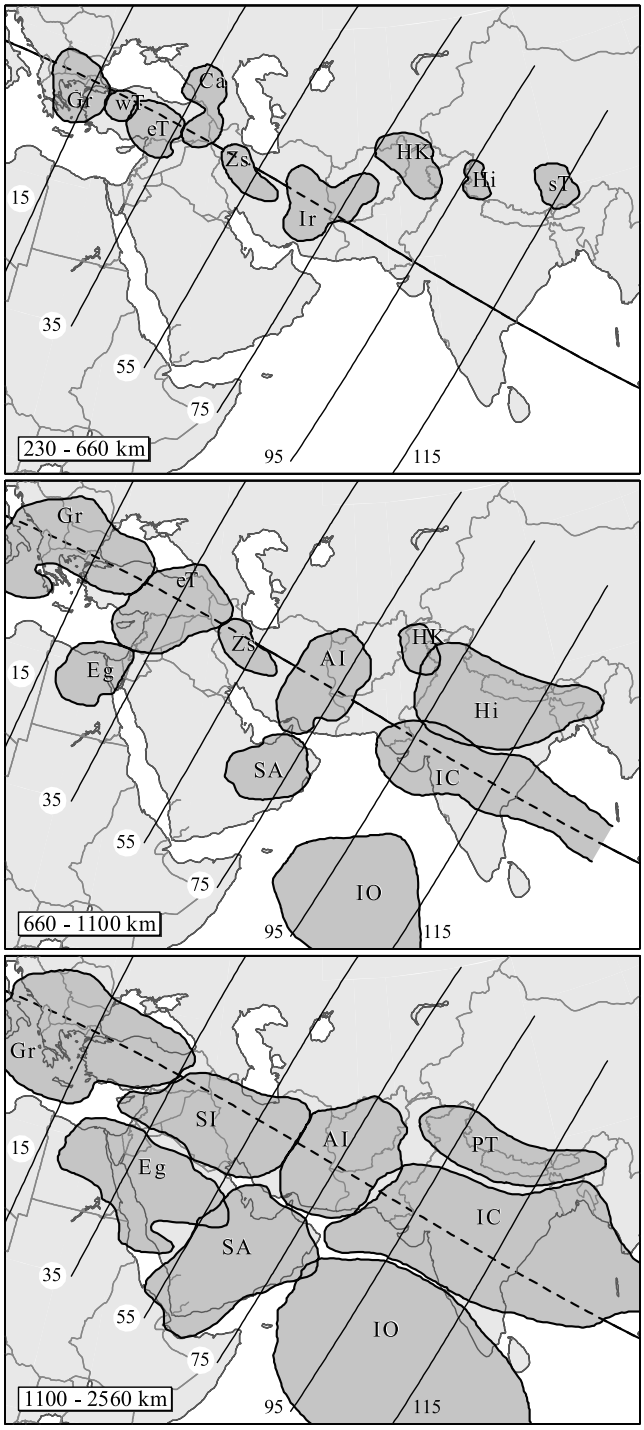

Figure 8. Horizontal overview of the tomographic anomalies that are considered to represent volumes of subducted Tethyan lithosphere in the depth intervals of (top) 230–660 km, (middle) 660–1100 km, and (bottom) 1100–2560 km. The contour line of each anomalous body is a projection of its maximum horizontal extent in the given depth interval. The lines and numbers indicate the vertical cross sections shown in Figure 5.

separate oceanic back-arc basins as well as active oceanic spreading during convergence may have added to the amount of subducted lithosphere, as will be discussed further below.

4.2. Definition of Initial Thermal Volumes of Subducted Lithosphere

[31] We approximate the initial thermal volume of subducted oceanic lithosphere by multiplying the calculated surface with an appropriate initial thermal thickness. In the likely case of a 30% amplitude underestimation in the tomographic inversion as discussed above, our tomographic volumes are bounded by velocity anomalies that can be associated with thermal perturbations of −143°C instead of −100°C. We therefore define the initial lithospheric thickness of the subducted oceanic plate surface as the age-dependent depth of the isotherm that differs −143°C from the ambient mantle temperature according to the plate cooling model of *Parsons and Sclater* [1977].

[32] Since we have no direct information on the lithospheric ages of the Tethyan lithosphere upon subduction, we have to approximate these. For each subduction scenario of Figure 3, we therefore reconstruct the simplified, temporal variation of the age upon subduction for each oceanic domain separately. When doing so, the proposed moments of oceanic rifting, initiation of subduction, ridge subduction, and final closure of each domain are acknowledged.

[33] Moreover, two possible scenarios for the spreading history of the Tethys Oceans are considered: In spreading scenario A, all oceanic spreading systems are assumed to remain active until the ridges are eventually subducted (Figure 10, left). This scenario will lead to relatively young ages of the subducting lithosphere. In spreading scenario B, spreading within the oceanic basins stops at the very moment the plate starts to subduct (Figure 10, right). This will result in relatively old lithospheric ages upon subduction.

[34] Whereas both spreading scenarios simplify the complicated evolution of the area to a 2D situation, and do not take into account the actual spreading velocities, they do provide a tool for analyzing the associated thermal volumes. In spreading scenario A, the relatively small thermal volume, determined for the continent-continent motions alone, represents only part of the total volume. The intrinsically assumed spreading of the lithosphere during convergence must have added to the total amount of subduction. As illustrated in Figure 10, the actual thermal volume in spreading scenario A may thus be similar or larger than that in scenario B. Although it can be difficult to distinguish between the two spreading scenarios in some cases, the difference between the thermal and tomographic volumes in spreading scenario A may thus provide us with an estimate of the amount of additionally subducted material.

[35] We use the average ages upon subduction of each oceanic domain to approximate the age and associated thickness of the subducted lithospheric surface. The reconstructed isochrons of *Stampfli and Borel* [2004] would allow for a more detailed assessment of these ages in the future. The average ages for the separate oceanic domains reconstructed here will be discussed below where appropriate. They vary from 35 to 185 Ma (average about 85 Ma), leading to values for the initial thermal thickness of the subducted lithosphere ranging from 75 to 110 km (average

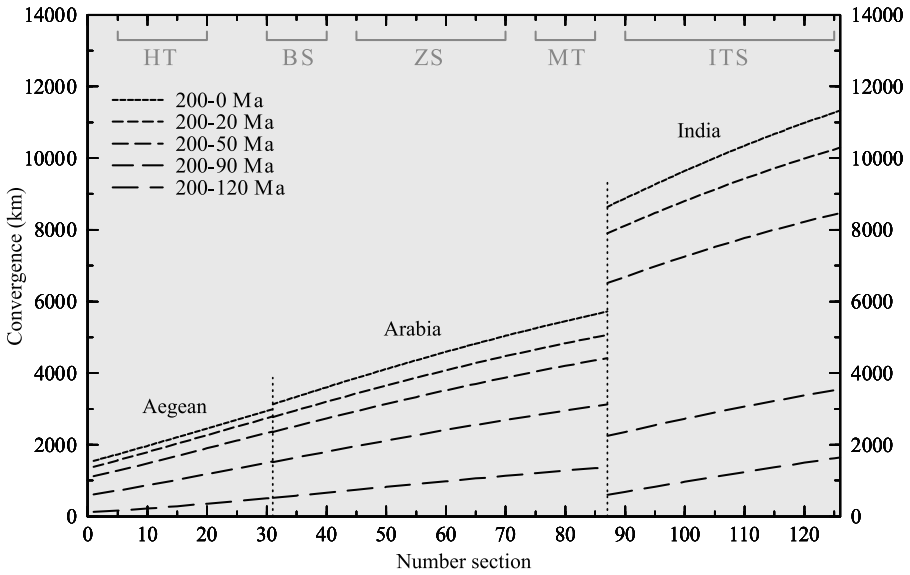

Figure 9. Total convergence per section between 200 Ma and the indicated time in the past. Tectonic features as in Figure 7 (bottom) are given for reference.

100 km). Hereafter, the initial thermal volumes of the subducted lithosphere are referred to as "Vi" (step 2 of Figure 1), with the two spreading scenarios providing upper and lower bounds on these volumes.

4.3. Prediction of Present Thermal Volumes of Subducted Slabs

[36] The present thermal signature associated with the slabs will differ from the original volumes of the subducted lithosphere because both the slab and the surrounding mantle temperatures have been affected during subduction. From the initial thermal volumes Vi of the subducted Tethyan lithosphere defined above, we will now predict the present thermal volumes, hereafter referred to as "Vp" (step 3 of Figure 1). Again, we will bound these volumes by perturbations of −143°C relative to the unperturbed mantle temperatures.

4.3.1. Evolution of Subduction Zone Temperatures

[37] The evolution of the temperatures in subduction zones is governed by thermal conduction, convection in the mantle wedge, phase transitions, and frictional heating at the plate

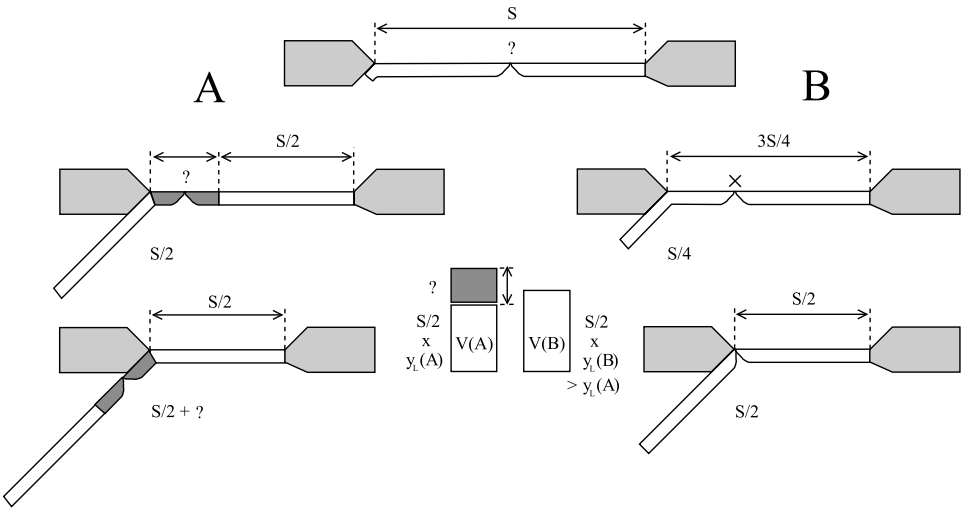

Figure 10. Two scenarios for the spreading history of the Tethys Oceans. (left) Spreading scenario A. The spreading system remains active until the ridge is subducted. The darker gray symbolizes the surface created since the plate started to subduct. (right) Spreading scenario B. Spreading stops at the very moment the plate starts subducting, as is symbolized by the X at the ridge. As the average lithospheric thickness y_L(A) is smaller than y_L(B), the thermal volume predicted from the continent-continent motions alone will be smaller for scenario A than for scenario B as well (thus V(A) < V(B) in bottom/middle columns). Because active oceanic spreading will have added to the total amount of subduction in scenario A, however, the actual thermal volume in this scenario may be larger than that in spreading scenario B, as illustrated by the darker gray, unknown volume.

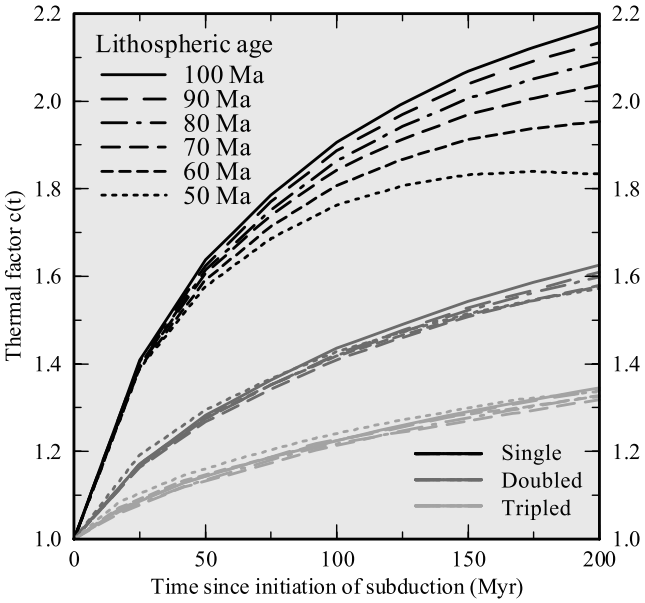

Figure 11. Anomaly evolution function $c(t)$ with which the initial thermal volumes will be multiplied to approximate the present thermal volumes of the subducted lithosphere: $c_1(t)$ for "single" cases (black lines) in which the slabs kept their plate-like geometry and $c_2(t)$ and $c_3(t)$ for "doubled" and "tripled" cases (grey lines) in which lithosphere is assumed to have experienced instantaneous pure shear thickening by a factor of 2 and 3. The time t since initiation of subduction (Myr) is used as the moment of initiation of Tethyan slab subduction before present (Ma). See text for further details and assumptions made.

contact. Reheating of the slab and associated cooling of the surrounding mantle therefore depends on several parameters, including the initial thermal structure, the convergence rate, and the residence time in the mantle. For actively subducting slabs, information on parameters like these can be reasonably well estimated. The present temperatures in these subduction zones can be approximated by numerically modeling the subduction process with the relevant parameters constraining the kinematic boundary conditions.

[38] As discussed earlier, detailed information on the parameters needed to directly model the subduction zone temperatures is relatively scarce for the Tethyan region. The large amount of subducted material (Figure 9) and its long residence time in the mantle form yet another complexity. Instead of actually modeling the evolution of the temperatures, we will develop an alternative method to approximate the present thermal signature of the Tethyan slabs: We will predict the present thermal volume Vp of each slab from its initial thermal volume Vi through $Vp = c(t) \cdot Vi$. The anomaly evolution function $c(t)$, displayed in Figure 11, will be determined on the basis of a wide range of numerical modeling results for the thermal evolution of subduction zones. The function will vary with, among others, the slab residence time in the mantle t, the lithospheric age upon subduction, and the amount of slab thickening.

4.3.2. Modeling Approach

[39] We analyze the evolution of subduction zone temperatures using the thermokinematic modeling procedure of *De Jonge et al.* [1994]. The approach is similar to the method developed by *Minear and Toksöz* [1970] and *Toksöz et al.* [1971, 1973]: The subduction process is modeled by shifting the initial temperatures stepwise into the mantle along a prescribed path, in combination with entrained mantle flow, with thermal diffusion calculated after each time step. Radiogenic heat production in the oceanic crust and mantle is ignored, and the phase transitions around the 410-km and 660-km discontinuities are modeled as abrupt temperature jumps of 90°C and −70°C, respectively. Boundary conditions for the model include a fixed 0°C at the top, a small constant heat flux into the base of the model, and no heat flow through the left and right sides of the model. The thermal effect of adiabatic compression in the convecting mantle is accounted for after the diffusion problem has been solved [*McKenzie*, 1970]. In addition to our subduction models for slabs of normal lithospheric thicknesses, we also model the subduction of slabs that have experienced pure shear thickening by a factor of 2 and 3, thus have doubled and tripled lithospheric thicknesses. For further details and values of the standard modeling parameters used, we refer to *De Jonge et al.* [1994].

4.3.3. Modeling Results

[40] From the modeled 2D thermal structures, we can determine the volumes in which the temperatures differ from the unperturbed, depth-dependent mantle temperatures by at least −143°C. These anomalous volumes will thus include the slab material itself as well as the thermally affected mantle material surrounding the slab. We now take these thermal anomalies as the modeled present volume V_p^m, and the volume associated with the same slab when not influenced by thermal diffusion as its modeled initial volume V_i^m, with the superscript m denoting the thermal modeling-based values. During ongoing subduction, when the amount of already subducted material is actually increasing, both V_p^m and V_i^m change with time. After subduction has ceased, V_i^m remains constant while V_p^m changes because the slab and mantle temperatures are further affected by thermal diffusion. The time for slabs to reach thermal equilibrium with the mantle by diffusion will significantly increase in case they are thickened.

[41] We model the evolution of subducting slabs for different lithospheric ages, rates of subduction and total evolution times t, and evaluate the parameter-sensitivity of $c^m(t)$ $(=V_p^m/V_i^m)$. Whereas the age dependence of V_i^m is straightforward, its importance for V_p^m (and thus $c^m(t)$) appears to depend on both the subduction rate and the total evolution time. The effects of the slab length and the values of the thermal conductivity, thermal expansion and dip angle were found to be relatively small. Our modeling results indicate that the values of V_p^m and $c^m(t)$ predominantly change directly after slab material enters an unperturbed mantle region for the very first time, and are only little affected by the slab part following later. This effect becomes stronger for an increasing factor of slab thickening. In fact, we found that only for small, active and unthickened slabs, the descent rate will significantly influence V_p^m and $c^m(t)$. As discussed earlier, most Tethyan slabs have been very large, have stopped to actively subduct and are probably thickened in the mantle. The effect of the subduction rate will thus be of relatively little importance when predicting the present thermal volumes for the Tethyan

region. For simplicity, we therefore determine $c^m(t)$ for a subduction model in which the slab volume V_i^m is placed into the mantle instantaneously at $t = 0$ after which it continues to warm up.

4.3.4. Anomaly Evolution Function

[42] Figure 11 shows the age-dependent variation of $c^m(t)$ for a subduction model in which oceanic lithosphere of 3000 km length, for three factors of thickening, is placed into the mantle instantaneously at $t = 0$. These modeling-based values of $c^m(t)$ will be used as the anomaly evolution function $c(t)$ for the Tethyan slabs in sections 5–7, with the modeling evolution time t as the residence time in the mantle. The anomaly evolution functions for slabs that have kept their plate-like geometry during subduction will be denoted $c_1(t)$ for "single" lithosphere in the following, while those for "doubled" and "tripled" lithosphere will be referred to as $c_2(t)$ and $c_3(t)$, respectively. Because both the residence time and amount of thickening in the upper mantle are unknown, we will use $c_2(t)$ and $c_3(t)$ for the whole slabs.

[43] As can be seen in Figure 11, $c_2(t)$ and especially $c_3(t)$ are much less sensitive to variations in the lithospheric age and residence time in the mantle than $c_1(t)$ is. When using values of $c_1(t)$ for the instantaneous subduction model of Figure 11 for slabs that have subducted at rates of ~3 cm/yr, we will generally underestimate their present thermal volumes Vp with 10–30% at most (namely, for $t = 200$ Myr). For $c_2(t)$ this will be at most 10%, whereas the difference will be negligible for $c_3(t)$. For very young (~25 Ma) oceanic lithosphere, the volumes of Vp will be underestimated even more, particularly for $c_1(t)$. For $c_2(t)$ and $c_3(t)$, they will be underestimated by at most 30% and 15%, respectively. The actual errors in our predicted thermal volumes will depend on the time of initiation of subduction, as well as that of the cessation thereof, and will strongly decrease with an increasing factor of thickening.

4.3.5. Mantle Residence Times of Tethyan Slabs

[44] For the subducted Tethyan lithosphere, we have now reduced the parameters needed to predict the present thermal volumes to (1) the average lithospheric age upon subduction, (2) the possible amount of slab thickening, and (3) the time since initiation of subduction. Whereas the time dependence of the anomaly evolution function decreases with increasing time and an increasing factor of slab thickening (see Figure 11), the choice of t is important in determining the finally predicted volumes. For each Tethyan oceanic basin separately, we will thus investigate when subduction thereof has started, and take the values of $c(t)$ for this particular time t since initiation of subduction to define the present Tethyan volumes Vp.

[45] In section 5, we will first analyze the Tethyan bulk volumes associated with the continent-continent motions alone. In this specific case, we will use values of $c(200)$ to predict the present thermal volumes of all slab material, implicitly assuming that it has been subducted as a single slab within the same region at $t = 200$ Myr before present. Evidently, however, the material has been subducted as separate slabs and in different parts of the mantle, leading to smaller residence times t, and thus smaller values for $c(t)$ and Vp as well. In other words, the thermal volumes predicted for the subducted material associated with the continent-continent motions in section 5 will provide upper limits of their actual volumes.

[46] In sections 6 and 7, we will use different residence times t, and thus different values of $c(t)$ from Figure 11, for all distinct stages of the subduction scenarios investigated. The effects of tectonic processes like continental collision, ridge subduction and slab detachment on the present thermal volumes of the subducted material, as well as the possible subduction of separate back-arc basins, will be addressed. Each time we expect material to be subducted as a new slab in relatively unperturbed mantle, we adjust t and $c(t)$ accordingly.

[47] The values of the residence times t used to predict the present thermal volumes for the separate oceanic domains reconstructed here will be discussed in the appropriate sections below. The values of $c_1(t)$ vary from 1.2 to 2.2, while those of $c_2(t)$ and $c_3(t)$ range from 1.1 to 1.6, and from 1.1 to 1.3, respectively. For a complete overview of the used values we refer to *Hafkenscheid* [2004].

5. First-Order Analysis of the Tethyan Bulk Volumes

5.1. Volume Estimates From Continental Convergence

[48] We first investigate the large-scale Tethyan evolution by analyzing the bulk volumes of lithospheric material subducted in the past 200 Myr according to the continent-continent motions alone. As mentioned in section 4, we assume that this total amount of convergence is the same for all three subduction scenarios of Figure 3 because the underlying tectonic reconstructions propose similar continent-continent motions. To predict the present thermal volumes of the subducted lithospheric surface, we use the average of the age of the oceanic lithosphere subducted since 200 Ma, and the age-dependent values of the anomalies evolution function $c(t)$ for $t = 200$ Myr (see Figure 11). The reconstructed variations in the lithospheric age upon subduction significantly differ for the three subduction scenarios, but the averages for scenarios I and II are found to be equal, and comparable to those for scenario III. The predicted thermal volumes are therefore similar for all three subduction scenarios accordingly. The bulk volumes predicted for the subducted material are shown in Figure 12, together with the total volumes of all relevant tomographic anomalies.

5.2. Comparison

5.2.1. Volumes

[49] As can be seen in Figure 12, the predicted thermal volumes for unthickened slabs are significantly larger than the tomographic volumes. For doubled or tripled slabs, however, the predicted volumes are equivalent to or somewhat smaller than the tomographic volumes. When comparing the predicted and tomographic volumes for the Aegean/Arabian and Indian regions separately (not shown here), their ratios are found to be similar to those for the total Tethyan region. This holds for all three factors of slab thickening and for both spreading scenarios. For the Tethyan region as a whole, as well as for the Aegean/Arabian and Indian regions separately, our results thus suggest that most Tethyan slabs have thickened in the mantle by a factor of 2 at least. As tentatively suggested by *Van der Voo et al.* [1999] already, this could be expected in view of the >10,000 km (Figure 9) of subducted lithosphere, which simply cannot have kept a plate-like

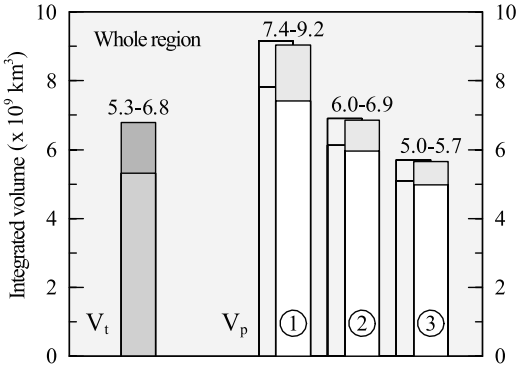

Figure 12. Total tomographic volumes (Vt) versus predicted thermal volumes (Vp) for the Tethyan region. The predicted thermal volumes are shown for spreading scenarios A and B, and for slabs that (1) have kept their plate-like geometry, (2) have thickened by a factor of 2, and (3) have thickened by a factor of 3. The values of Vp in the front are representative for subduction scenarios I and II, and those in the background are representative for subduction scenario III.

geometry in the mantle, and the bulk volumes of the seismic anomalies. As discussed in section 4, the thermal volumes predicted with our approach are typically underestimates of the actual volumes because they are based on the modeling results for instantaneously subducted slab material. Simultaneously, however, the volumes are likely to be overestimates of the actual volumes because they are here predicted using values of $c(200)$. The relative contributions of these two aspects are probably on the order of 10% for doubled slabs, but much less for tripled slabs, and may well compensate each other. In any case, we expect more convergence (thus more lithospheric material to be subducted) than calculated for the continent-continent motions alone.

5.2.2. Trench-Normal Distribution

[50] Because recent Cenozoic subduction in the Tethyan region has been in a primarily northward to northeastward direction, the tomographic anomalies associated with these young slabs are likely to be found in the upper mantle underneath, or just north, of the present subduction and suture zones. We expect that the material subducted further back in time can be found south to southwest of this area, and deeper in the mantle, because the absolute locations of the continents as well as the relative locations of the trench systems prior to the continental collisions have been more south to southwest as well. The positions of the several tomographic anomalies are indeed in accordance with these expectations (e.g., see Figure 8 and *Van der Voo et al.* [1999]).

5.2.3. Trench-Parallel Distribution

[51] Both the tomographic volumes and the predicted thermal volumes gradually increase along the Tethyan trench system from west to east (Figure 13). The tomographic volumes seem to be more or less continuous along the trench system in the Aegean and Arabian regions, which is probably related to that fact that the Arabian and African plates have moved together before separating around 30 Ma. We will therefore present the volumes belonging to the Aegean and Arabian regions together in the following. More eastward, the trend shows an abrupt jump toward the Indian tomographic volumes. Clearly, the large strike-slip motion of the Indian plate relative to the African-

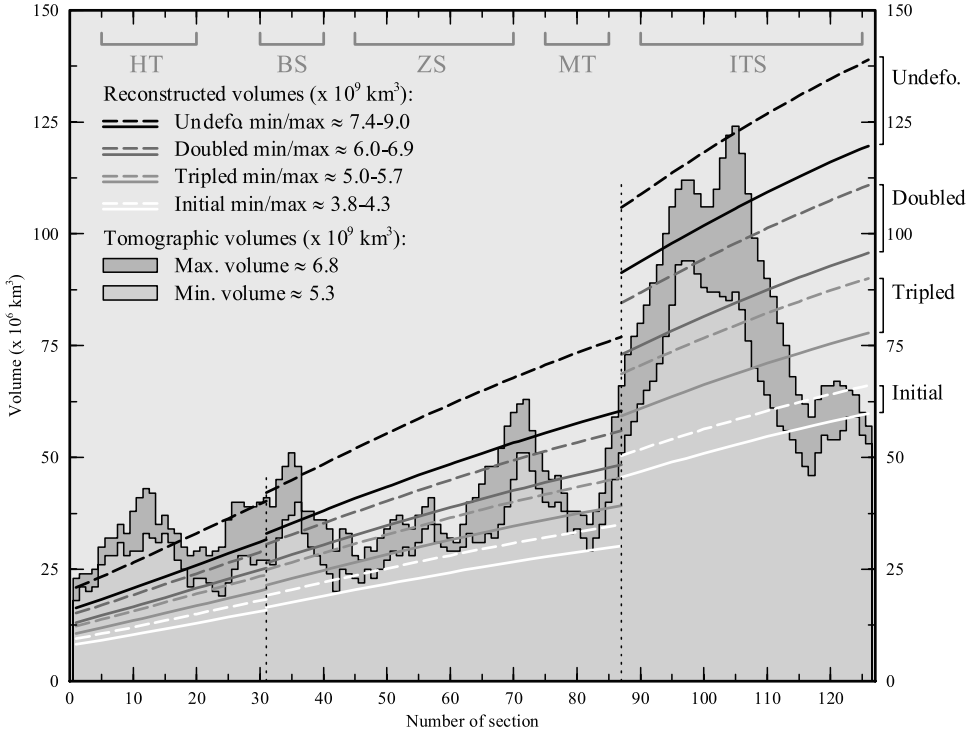

Figure 13. Tomographic volumes versus predicted (initial and present) thermal volumes throughout the Tethyan region. The present thermal volumes are shown for slabs that have kept their plate-like geometry (undeformed), have thickened by a factor of 2 (doubled), and have thickened by a factor of 3 (tripled).

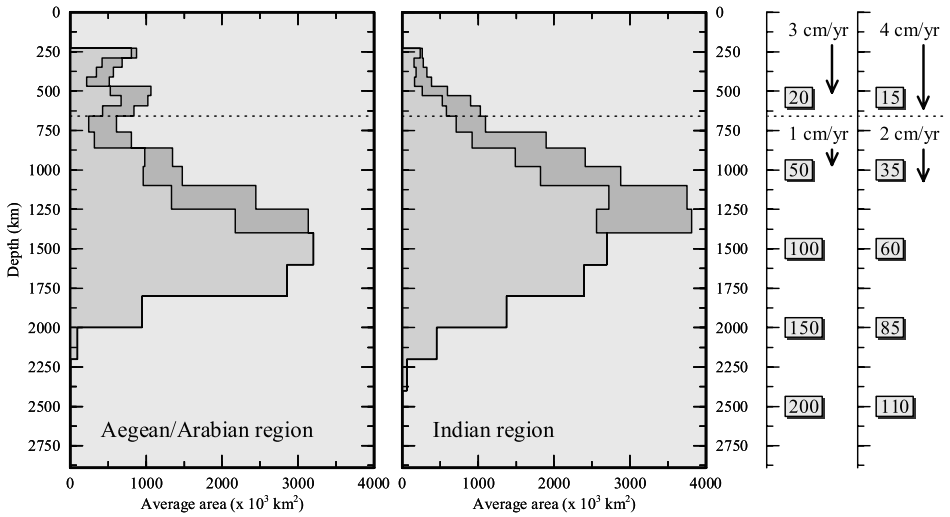

Figure 14. Vertical distribution of the tomographic volumes for the Aegean/Arabian and Indian region separately. On the right, the approximate time (Myr) needed for subducting material to reach the shown depths when moving with a vertical rate of 3–4 cm/yr in the upper mantle and 1–2 cm/yr in the lower mantle is shown. The integrated volumes below 1400 km depth are similar for both regions. Between 800 and 1400 km depth, the Aegean/Arabian volumes are two thirds of the Indian volumes.

Arabian plate during the Mesozoic and Cenozoic must have influenced the process of subduction here. The Owen Fracture Zone, associated with this motion and chosen to split up the Arabian and Indian region, is indeed parallel to the boundary between the lower mantle anomalies in the Middle East and those in the Indian region (cf. Figures 4 and 5). The tomographic volumes shown in Figure 13 decrease again east of section 115. Whereas the deep mantle anomalies extend along the whole Indian trench system, and even farther eastward to the Indonesian archipelago (see Figure 4), the tomographic volumes have their major bodies in the western part of the Indian region. The drop in total volume per section is almost as clear as the one on the western side of the area, suggesting a comparable geodynamic cause.

5.2.4. Depths

[52] In Figure 14, the vertical distribution of the tomographic volumes is plotted for the Aegean/Arabian and the Indian regions separately. With a vertical component of the subduction rate of ~1 cm/yr in the lower mantle (see section 2), a 150-Myr time span must have been enough for the subducted material to have reached the ~2000 km depths of the anomalies found in the tomographic model. If this has been the case, the difference in Aegean/Arabian and Indian volumes between 800 and 1400 km depth could be related to the relatively large amount of subduction in the Indian region between 90 and 20 Ma. In view of the fast subduction in the Indian region, however, vertical subduction rates through the lower mantle may have been higher, and the above mentioned depths may have been reached in a shorter time span accordingly. More specifically, a 2 cm/yr vertical rate would require the material subducted prior to 80–90 Ma to have flattened and piled up above the 2000 km depth. This plausible option will be discussed in more detail in section 6.

5.3. Conclusions

[53] Our approach is used here to evaluate the bulk volumes of subducted lithosphere associated with the continent-continent motions in the Tethyan region. We find that the volumes, locations and depths of the tomographic anomalies are in accordance with our general predictions. The present thermal volumes of subducted lithosphere are in agreement with the tomographic bulk volumes when Tethyan slab thickening by at least a factor of 2 is taken into account. This also means that all tomographic volumes analyzed here are likely to be related to the subducted Tethyan lithosphere. Because the first-order continent-continent motions are similar for all three subduction scenarios (Figure 3), we cannot distinguish between the underlying reconstructions on the basis of this analysis. In sections 6 and 7, we will use more specified predictions of the present thermal volumes to investigate the Tethyan evolution and the differences between the subduction scenarios and tectonic reconstructions in more detail.

6. Slab Volumes After Subduction of Oceanic Ridges and Back-Arc Basins

[54] As discussed in section 2, the anomalous volumes associated with the leading and trailing oceanic lithosphere around a subducted spreading center may be imaged as two separate volumes in the tomography model. Also the slabs of separate oceanic back-arc basins may be visible as distinct anomalous volumes in the tomographic images.

6.1. Volume Estimates

[55] As the subduction scenarios discussed in section 2 encompass different histories for the subduction of the Neo-Tethyan ridge and separate oceanic basins, we expect different divisions of the thermal volumes as well. We will here assume that the thermal volume associated with the subducted Neo-Tethyan lithosphere has split into two subvolumes at the time of ridge subduction according to each scenario. The volumes subducted before and after ridge subduction will be referred to as BRS and ARS, respectively. As a result of the subdivision, the average ages of the lithospheric basins and their total residence times t in the

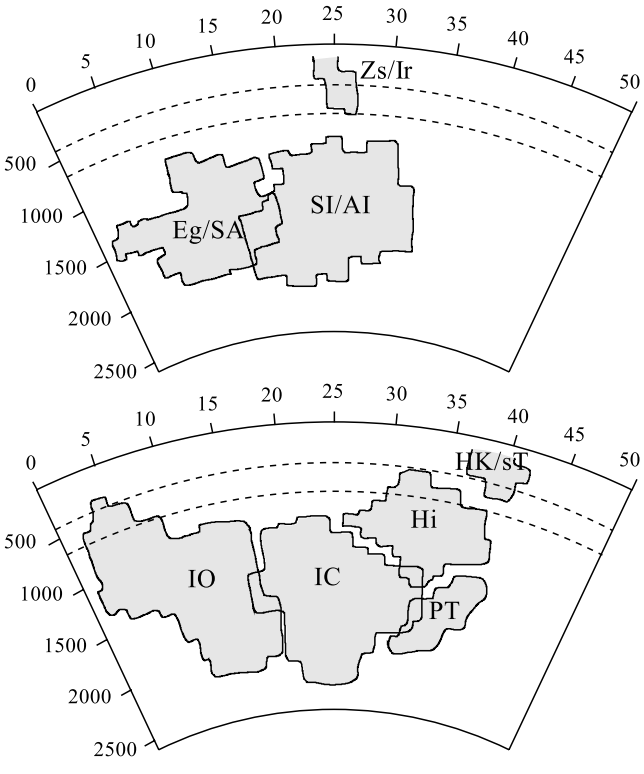

Figure 15. Vertical overview of the tomographic anomalies associated with subducted Tethyan lithosphere in (top) the Arabian region and (bottom) the Indian region. The contour line of each anomalous body is a projection of its maximum extent approximately for cross sections 40–80 in the Arabian region and cross sections 90–120 in the Indian region (see Figures 7 and 8).

mantle will change significantly, and thus the predicted thermal volumes accordingly. For both the Semail and Spongtang back-arc basins of subduction scenario III, we separately assess the total surface subducted and average lithospheric age upon subduction below. Subduction of these basins is assumed to have started at the moments of obduction onto the southern continental margins, i.e., at t = 80 Ma and 65 Ma in the Arabian and Indian regions, respectively.

6.2. Approach of Analysis

[56] We evaluate the merits and shortcomings of the three subduction scenarios by analyzing, for the Arabian and Indian regions separately:

[57] 1. The relative distribution of the subvolumes as predicted for each subduction scenario and illustrated in Figure 3. Analogous to the geographical distribution of the seismic anomalous bodies (Figure 8), we have plotted the vertical extents of these volumes in two bands of cross sections in Figure 15.

[58] 2. The past locations of subduction, as inferred from the plate motions in the absolute frames of reference discussed in section 2, compared to the positions of the tomographic anomalies. Figure 16 shows the possible locations of the continental margins around 80 Ma and 65 Ma, the proposed moments of Neo-Tethyan disappearance and obduction.

[59] 3. The agreement between predicted thermal volumes and tomographic volumes, for both spreading scenarios, all three factors of slab thickening, and all three subduction scenarios (see Figures 17 and 18). We expect an additional amount of subducted material due to active oceanic spreading in the Neo-Tethys during its subduction.

[60] 4. The timing of subduction versus the depth ranges of the relevant tomographic anomalies. We will consider descent rates of 3–5 cm/yr in the upper mantle, and 1–2 cm/yr in the lower mantle, as discussed earlier.

[61] We recall the conclusions from our first-order analysis of the Tethyan bulk volumes that (1) slab thickening by at least a factor of 2 has to be taken into account and (2) all tomographic volumes are needed to accommodate the predicted thermal volumes. Only in the Indian region, we will assume that the lower mantle anomaly PT (e.g., see

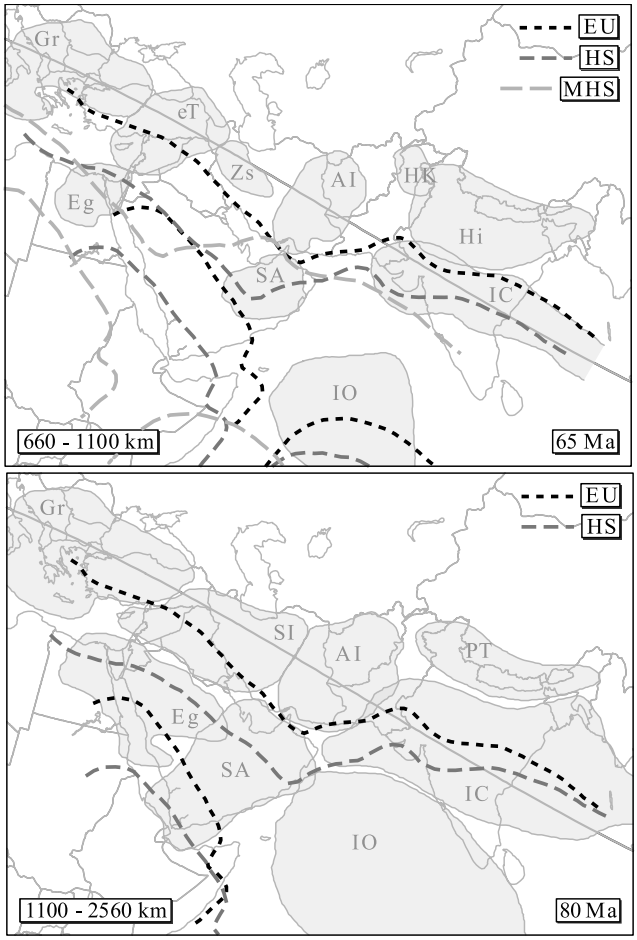

Figure 16. Past locations of the southern continental margin of Eurasia and the northern continental margins of Arabia and India [*Norton*, 1999] with Eurasia fixed (EU), in a fixed hot spot reference frame (HS) [*Duncan and Richards*, 1991; *Müller et al.*, 1993], and in a moving hot spot reference frame (MHS) [*O'Neill et al.*, 2003]. Also shown are the tomographic anomalous bodies associated with subducted Tethyan lithosphere. Present coast lines and political borders are given for reference only. (top) Absolute locations at 65 Ma with tomographic anomalies in the 660–1100 km depth interval. (bottom) Locations at 80 Ma with anomalies in the 1100–2560 km depth interval.

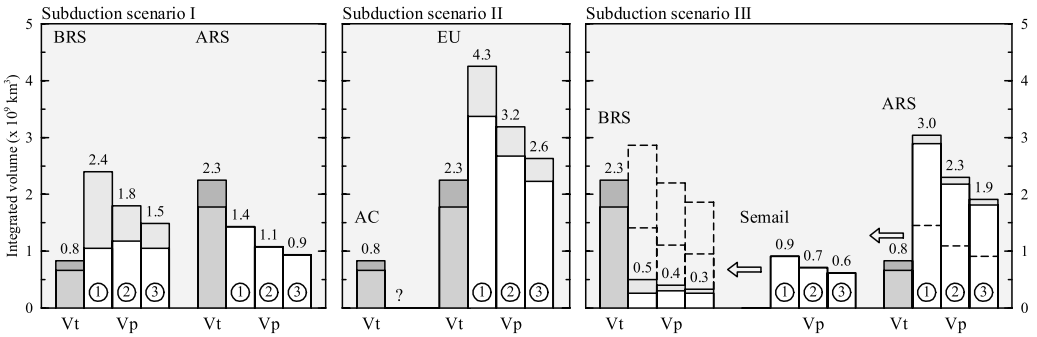

Figure 17. Tomographic volumes versus predicted thermal volumes for the Arabian region (cf. Figure 12). (left) Subduction scenario I, volumes divided into parts associated with subduction before Neo-Tethyan ridge subduction (BRS) and after ridge subduction (ARS). (middle) Subduction scenario II, volumes divided into parts associated with subduction near the Arabian continental margin (AC) and underneath Eurasia (EU). (right) Subduction scenario III, volumes divided into parts associated with Neo-Tethyan BRS and ARS subduction (see above), as well as a separate part associated with subduction of the Semail back-arc ocean. The arrows indicate that the predicted Semail volume and half of the predicted ARS volume may be incorporated in the predicted BRS volume.

Figure 15) represents remnants of subducted Paleo-Tethyan lithosphere, as proposed earlier by *Van der Voo et al.* [1999]. The modest size of this anomaly, however, suggests that the larger part of the Paleo-Tethyan lithosphere is not detectable by tomographic means at present, or should be found elsewhere. The deep lower mantle anomalies underneath central Asia referred to in section 3 (see Figure 4, bottom) may well represent the remaining remnants of Paleo-Tethyan lithosphere. We further note that subduction scenario II is proposed only for the Arabian region.

6.3. Arabian Region

6.3.1. Subduction Scenario I

[62] For subduction scenario I, with Neo-Tethyan ridge subduction around 80 Ma, we expect two subvolumes of slab material that are both subducted relatively close to the present Zagros suture zone.

[63] For this scenario, we select the southern anomalies Eg/SA as BRS volumes, and the remaining, northern anomalies as ARS volumes (Figures 15 and 16). As can be seen in Figure 16, however, the southernmost anomalies of Eg/SA are too far south to be explained properly by subduction at the Eurasian continental margin alone as proposed by subduction scenario I.

[64] Figure 17 (left) shows that the predicted BRS volumes are larger, and the predicted ARS volumes much smaller, than the associated tomographic volumes for this subduction scenario. The BRS volumes predicted for spreading scenario A are comparable to the tomographic volumes, but probably underestimated by 15–30% owing to the relatively young lithospheric age of this basin (section 4). A possible solution to the discrepancy between predicted and tomographic volumes would be to let the ridge subduct earlier in time so that the predicted volumes for BRS will become smaller and those for ARS larger. However, to change the calculated thermal volumes significantly, a larger time shift is necessary than that is justified by the reconstructions followed here [*Şengör and Natal'in*, 1996; *Norton*, 1999].

[65] Anomalies Eg/SA, identified as the older BRS volumes for this subduction scenario, can be found mainly in the ~800 to 2000 km depth range (Figure 15, top). The younger ARS volumes of SI/AI, however, are positioned

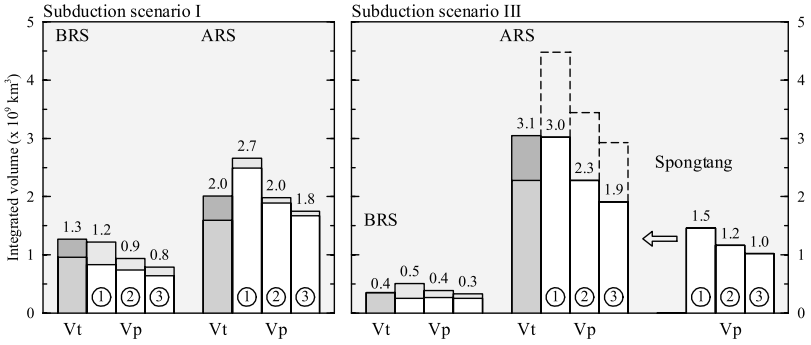

Figure 18. Tomographic volumes versus predicted thermal volumes for the Indian region as in Figure 17. (left) Subduction scenario I. (right) Subduction scenario III. The separate part is now associated with subduction of the Spongtang back-arc Ocean. The arrow indicates that the predicted Spongtang volume may be incorporated in the predicted ARS volume. Subduction scenario II is proposed only for the Arabian region.

deeper, with a relatively large part between 1400 and 2200 km depth. The deep position of anomalies SI/AI can only be explained by subduction of the associated ARS volumes after 80 Ma if we assume vertical subduction rates of about 4 cm/yr in the upper mantle and 2 cm/yr in the lower mantle. On the contrary, the top of Eg/SA around 800–1000 km is in accordance with subduction of the associated BRS volumes prior to 80 Ma only if we adopt vertical subduction rates of ~1 cm/yr instead. Although somewhat speculative, the fit of this subduction scenario to the depth intervals of the several tomographic anomalies is not very satisfactory.

6.3.2. Subduction Scenario II

[66] For subduction scenario II, we expect the subvolume possibly accommodated at the Arabian continental margin (AC) around 80 Ma to be only very small, and basically all Neo-Tethyan (N-T) lithosphere to be subducted as one single volume underneath the Eurasian margin (comparable to subduction scenario I).

[67] For this scenario, the small slablet AC could be associated with the southern anomalies Eg/SA, or only the southernmost parts of these, in both reference frames of Figure 16 (bottom). The remaining, northern anomalies are thus selected as N-T lithosphere. To explain the positions of the northern part of Eg/SA by subduction along the Eurasian margin (see further discussion below), the HS reference frame seems to be needed.

[68] To explain the tomographic volumes of Eg/SA, associated with the slablet AC in this scenario, the originally subducted surface must have been relatively large and similar to the surface subducted in the Arabian region between 90 and 50 Ma (for calculations, see *Hafkenscheid* [2004]). For the elongated Arabian continental margin, such a surface would require about ~1000–2000 km of subduction (Figure 9), which does not seem to be justified by the underlying tectonic reconstructions [*Dercourt et al.*, 1993; *Şengör and Natal'in*, 1996]. Moreover, the predicted N-T volumes fit the associated tomographic volumes only if the slabs have thickened by a factor of 3 and for spreading scenario A (Figure 17, middle). This means that all additional N-T material created by the active oceanic spreading during convergence of this spreading scenario (see Figure 10) must have been accommodated elsewhere, and probably in the northern part of anomalies Eg/SA. In that case, only the southern part of these anomalies needs to be explained by the AC slablet.

[69] The southernmost anomalies of Eg/SA can all be found below 1200 km depth (Figure 15, top). These depths can be reached in ~80 Myr if vertical subduction rates have been 3 cm/yr in the upper mantle and 1 cm/yr in the lower mantle. This time span would be in agreement with the subduction of the slablet AC along the Arabian continental margin around 80 Ma proposed for this subduction scenario. The ≥2000 km depth of anomalies SI/AI can be reached in ~160 Myr with the same descent rates, which is a somewhat large time span in view of the small amount of convergence before 120 Ma (see Figure 9) but seems reasonable.

6.3.3. Subduction Scenario III

[70] We expect three separate thermal volumes for subduction scenario III, namely, (1) a Neo-Tethyan BRS part subducted beneath the Eurasian margin, (2) the remaining Neo-Tethyan ARS part subducted near the Arabian continental margin, and (3) the slab of the Semail back-arc Ocean subducted underneath Eurasia again. As the Semail Ocean is proposed to have overridden the complete Neo-Tethys between 140 and 80 Ma, we assume that the maximum size of this basin equals the surface constructed from the Arabia-Eurasia convergence between 80 Ma and the approximated onset of continental collision at 22 Ma (see Figure 9).

[71] Although the hot spot reference frame is uncertain prior to 84 Ma, we assume that subduction of the BRS volumes around 120 Ma in this scenario occurred somewhere above anomalies SI/AI (not shown here). Semail back-arc spreading will have resulted in ARS subduction much farther south (compare Figure 3), with a southernmost extent around the position of the Arabian continental margin at 80 Ma. As already discussed for subduction scenario II, both reference frames shown in Figure 16 (bottom) suggest that this location was above the southern anomalies Eg/SA. Subsequent subduction of the Semail Ocean must have been accommodated in SI/AI again, along the northward moving Eurasian margin. For subduction scenario III, the Neo-Tethyan lithosphere overridden by the Semail Ocean (ARS) is thus associated with the southern anomalies Eg/SA. The oldest Neo-Tethyan slab (BRS) and the Semail remnants are associated with the remaining, northern tomographic volumes. Because the Neo-Tethyan lithosphere gradually disappeared underneath the spreading Semail back-arc basin in this subduction scenario, the slab may have flattened out under the full width of the basin, as discussed in section 2. If the Neo-Tethyan slab has flattened, the oldest part of the ARS volume may have been incorporated in the northern lower mantle anomalies SI/AI, and only its younger part in the southern anomalies Eg/SA (see Figure 15).

[72] Figure 17 (right) shows that for subduction scenario III, the predicted volumes for the BRS group and Semail Ocean together are much smaller than the selected tomographic volumes. Although the predicted BRS volumes are probably underestimated in spreading scenario A because of the young age of the oceanic basin, even with the possible increase of 15–30% for thickened slabs the difference remains. Simultaneously, however, the predicted ARS volumes are much too large to be explained by the selected anomalies Eg/SA alone. If the Neo-Tethyan slab has flattened, as discussed above, anomalies SI/AI may represent not only the BRS and Semail volumes but also the oldest part of the ARS volume. In that case, only the youngest ARS part has been accommodated in Eg/SA. By equally dividing the predicted ARS volume over the tomographic BRS and ARS volumes, the balance between predicted and tomographic volumes improves. Evidently, the precise distribution is unknown, and a somewhat larger part of the predicted ARS volume may have been subducted in the northern part of the region just as well. In such a flattening scenario, the apparent separation between anomalies Eg/SA and SI/AI is not related to ridge subduction and must have another origin.

[73] As mentioned above, the ≥2000 km depth of anomalies SI/AI could be reached in ~160 Myr for vertical subduction rates of ~3 cm/yr in the upper and 1 cm/yr in the lower mantle. This would be in agreement with the

associated subduction of ARS material prior to 140 Ma. For the same rates, also the depths of the other anomalies seem to be in general agreement with subduction scenario III: First, the major bodies of anomalies SI/AI between 1100 and 2000 km depth need descent times of ~70–160 Myr, which would be in accordance with subduction between 140 and 80 Ma. Second, the ~800 to 1000 km deep top of anomalies Eg/SA requires descent times of ~40–60 Myr, which is only little shorter than expected for subduction prior to 80 Ma. The somewhat deeper position of the eastern anomaly SA with respect to the western anomaly Eg (e.g., see Figure 5) may reflect the diachronous subduction of the Neo-Tethys underneath the Semail Ocean. Finally, the tomographic upper mantle anomalies and the uppermost (<1100 km) anomalies of AI are likely to represent remnants of the Semail lithosphere subducted since 80 Ma.

6.4. Indian Region

6.4.1. Subduction Scenario I

[74] Analogous to the Arabian region, we expect two subvolumes of Neo-Tethyan lithosphere subducted close to the present Indus-Tsangpo suture zone for subduction scenario I.

[75] In the Indian region, the absolute locations of Eurasia have been much too far north to explain the positions of the southernmost tomographic anomalies by subduction at the Eurasian continental margins alone (Figure 16). Nonetheless, we need all major tomographic anomalies to accommodate the predicted thermal volumes. We will therefore compare the predicted BRS volumes to anomaly IO, and the predicted ARS volumes to the remaining tomographic volumes, anyway. Hi and IC have been identified as separate anomalies because their geometries and positions clearly differ (e.g., see Figure 4), but they represent a single oceanic basin in this subduction scenario.

[76] Subduction scenario I seems to adequately predict the subdivision of the volumes for the Indian region (Figure 18, left). The predicted BRS volumes for thickened slabs are smaller than the tomographic volumes. This allows for the additional subduction caused by the expected oceanic spreading during convergence, although it has to be acknowledged again that the predicted BRS volumes may be underestimated with 15–30% for spreading scenario A. For the ARS group, the predicted volumes are similar to the tomographic volumes if the slabs have thickened by a factor of 2 or 3.

[77] Anomaly IO, selected as BRS volume, can be found in a large depth interval but mainly between 800 and 2000 km depth (Figure 15). Very slow descent rates (~1 cm/yr) are required to make the top of anomaly IO fit to subduction of the BRS material prior to the 80 Ma proposed in this scenario. Remarkably, the most shallow parts of IO (in the upper mantle but mainly around 800 km depth, see Figure 4 also) are found furthest south, thus far away from the Eurasian continental margins. Anomaly IC of the younger ARS group is positioned between 1000 and 2200 km depth, which is even deeper than IO of the older BRS group (see Figure 15). Only with faster descent rates of ~2 cm/yr in the lower mantle, this deep level can be reached within the ~80 Myr expected for the subduction of the ARS material. As slabs have been found to descend faster in regions with abundant subduction in the same area (section 2), the relatively high convergence velocities between 90 and 50 Ma in the Indian region (Figure 9) may well have led to these faster descent rates. Nevertheless, such rates are in contradiction with the slower rates needed to explain the depth of anomaly IO.

6.4.2. Subduction Scenario III

[78] For subduction scenario III, we expect three separate thermal volumes as discussed above for the Arabian region. In the Indian region, we approximate the maximum size of the Spongtang Ocean by the surface constructed from the India-Eurasia convergence between 65 Ma (the start of its subduction) and 48 Ma (the onset of India-Eurasia continental collision).

[79] For this scenario, we consider the possibility that the Neo-Tethyan BRS volume, subducted prior to 120 Ma, is represented by the deepest part of the large tomographic anomaly IC. Analogous to the Arabian region, the southward migrating Spongtang back-arc Ocean may have caused the Neo-Tethyan ARS slab to flatten out over the full width of anomalies IO and IC between ~120 and 65 Ma (see Figures 15 and 16). The ARS volume is therefore coupled to both lower mantle anomalies, even though they seem to be separated in the tomographic images. Around 65 Ma, the Indian continental margin is positioned right above the southernmost, shallow anomalies of IO in all three reference frames (Figure 16). We note that the EU and HS frames seem to predict India somewhat too far east, and the MHS frame too far west instead. Also *Van der Voo et al.* [1999] suggested that obduction onto the northern Indian margin has been responsible for these southernmost anomalies. Finally, the shallower lower mantle anomaly Hi, underneath the present Indus-Tsangpo suture, may be identified as the separate Spongtang oceanic lithosphere.

[80] The predicted BRS volumes, subducted prior to 120 Ma in this scenario, are small (though somewhat underestimated owing to the young lithospheric age of the basin). They can be used to explain the deepest, 1800–2200 km part of anomaly IC (Figure 18, right). The predicted ARS volumes are smaller than the remaining tomographic volumes. If the subducted slabs have thickened by a factor of 3, the additional volume that was predicted for the Spongtang oceanic basin can be incorporated in these anomalies as well. Because of the relatively old age of the subducted ARS lithosphere, the predicted thermal volumes for spreading scenarios A and B are similar.

[81] As discussed in section 5, a 2 cm/yr descent rate in the lower mantle seems most likely for the Indian region if the slab material subducted prior to 90–80 Ma has flattened and piled up above 2000 km depth. For subduction scenario III, we do propose such large-scale flattening. Moreover, with a descent rate of 2 cm/yr in the lower mantle, the 1400 km depth of anomaly Hi (Figure 15) will have been reached in a total 50–60 Myr. While this relation has been pointed out already by *Van der Voo et al.* [1999] and *Replumaz et al.* [2004], we propose here that, for subduction scenario III, the estimate is in agreement with the subduction of the Spongtang basin since ~65 Ma. The shallow top of anomaly IO still requires locally slow descent rates. However, in subduction scenario III it needs to be explained by subduction prior to ~65–50 Ma only,

whereas in subduction scenario I this needed to be done by subduction prior to 80 Ma.

6.5. Summary

[82] For the three subduction scenarios illustrated in Figure 3 we summarize here the main findings.

6.5.1. Subduction Scenario I

[83] The tomographic volumes in the Arabian and Indian region can be explained by subduction scenario I if the N-T slabs have thickened by a factor of 2 at least. However, in all three reference frames considered here, the southernmost lower mantle anomalies are positioned too far south to be explained by subduction at the Eurasian continental margin alone. Furthermore, the relative distribution (in the Arabian region) and present depths of the tomographic anomalies (in both regions) cannot be well explained by subduction scenario I.

6.5.2. Subduction Scenario II

[84] Subduction in scenario II (for the Arabian region only) is predicted at the right absolute locations, as opposed to that in subduction scenario I. However, the size of the southernmost tomographic anomalies requires a significant amount of subduction at the Arabian continental margin around 80 Ma. We find that subduction scenario II can only explain the tomographic volumes if (1) the N-T slabs have thickened by a factor of 2 at least, (2) the Eurasian continental margin has been as far south in late Mesozoic times as suggested by the fixed hot spot reference frame of *Müller et al.* [1993], and (3) the convergence accommodated at the Arabian continental margin has been larger (on the order of 1000 km) than justified by the tectonic reconstructions underlying this subduction scenario.

6.5.3. Subduction Scenario III

[85] Because subduction scenario III includes the opening of a large back-arc oceanic basin at the Eurasian continental margin in the Arabian as well as the Indian region, it is least sensitive to the exact position of Eurasia. This subduction scenario can well explain the absolute locations of the tomographic anomalies in all three reference frames considered here. Moreover, the scenario predicts thermal volumes, including those of the separate Semail and Spongtang oceanic basins, that are in agreement with the tomographic volumes if (1) the N-T and back-arc slabs have thickened by at least a factor of 2 and 3, respectively, and (2) trench migration due to Semail and Spongtang back-arc spreading has caused extensive flattening of the overridden N-T slabs.

6.6. Conclusions

[86] For the Indian region, our analysis shows that subduction scenario III, based on the most recent reconstruction of *Stampfli and Borel* [2004], best describes the Mesozoic-Cenozoic subduction of the Tethys Oceans. For the Arabian region, the relative small distances between the Arabian and Eurasian continental margins make it difficult to distinguish between subduction scenarios II and III. Our analysis shows, however, that subduction scenario II is quite sensitive to the exact reference frame and requires additional constraints that seem to be in contradiction with the tectonic reconstructions underlying the scenario [*Dercourt et al.*, 1993; *Şengör and Natal'in*, 1996]. We therefore prefer subduction scenario III for the Arabian region as well. It thus appears that the tectonic reconstruction that explicitly incorporated the evolution of the plate boundaries through time can best explain the tomographic anomalous volumes associated with subducted Tethyan lithosphere.

7. Slab Detachment After Cenozoic Continental Collisions

[87] We investigate here if and when slab detachment can have occurred in response to the Cenozoic continental collisions and whether we are able to identify the associated subvolumes of slab material. According to *Van de Zedde and Wortel* [2001], convergence velocities of ~3 cm/yr as in the Arabian region (Figure 9) are likely to cause subducting slabs to break off ~10 Myr after the onset of continental collision (c.q. subduction of continental lithosphere). The high convergence velocities of the Indian region (>6 cm/yr, see Figure 9) can lead to slab break off after a delay time of only ~5 Myr. We will assume that slab break off has occurred at the above mentioned delay times at a 300 km downdip distance from the trench, which corresponds to a depth of about 100 km [*Van de Zedde and Wortel*, 2001]. The detached volumes of lithospheric material are further assumed to have sunk into the mantle vertically.

7.1. Timing Collision and Slab Break Off

[88] Starting with continental collision times of 22 Ma in the Arabian region and 48 Ma in the Indian region, as discussed in section 2, we first assume the slabs to have broken off around 12 Ma and 43 Ma, respectively. Although these break off times are in agreement with other studies [e.g., *Chung et al.*, 1998; *Kohn and Parkinson*, 2002; *Keskin*, 2003], the somewhat lower convergence velocities in the western parts of both regions could have led to a later break off locally. Especially for the Indian region there is evidence for diachronous slab detachment, with break off times in the western Himalayas around 20 Ma [e.g., *Chung et al.*, 1998; *Kohn and Parkinson*, 2002; *Mahéo et al.*, 2002]. Furthermore, an earlier onset of continental lithospheric subduction around 40–30 Ma in the Arabian region, as suggested by *Dercourt et al.* [1993] and *Jolivet and Faccenna* [2000], could have led to subsequent slab detachment around 30–20 Ma already. We will investigate the consequences of these possible alternative break off times further below.

7.2. Volume Estimates

7.2.1. Volumes Left Attached to the Surface

[89] For both regions, we isolate the tomographic volumes in the upper mantle that are completely detached from the volumes deeper in the mantle. We interpret the upper mantle volumes (Ca/Zs/Ir/HK/sT of Figure 8) as the material still attached to the surface after slab break off, or subducted thereafter, and will refer to them as AB in the following. Only the three upper mantle anomalies in the Aegean and westernmost Arabian regions (Gr/wT/eT of Figure 8) are continuous to their lower mantle volumes (e.g., see section 15 in Figure 5) and thus not incorporated in the AB volumes.

[90] For the predicted thermal volumes we select the associated AB volumes by omitting the lithosphere that we expect to haven broken off after continental collision. The lithospheric surface associated with the AB volumes

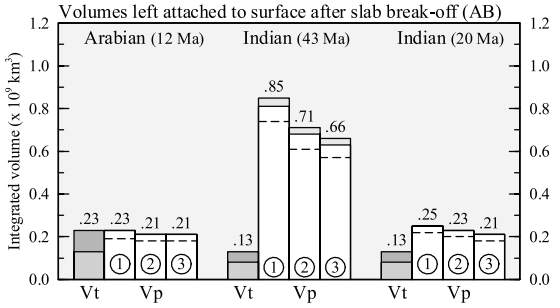

Figure 19. Tomographic volumes versus predicted thermal volumes assumed to be still attached to the surface after slab break off (AB). Break off is assumed to have occurred at 12 Ma in the Arabian region and at 43 Ma or 20 Ma in the Indian region. The predicted volumes are given for subduction scenario I (∼II), while the dotted lines indicate the values for subduction scenario III. The volumes are corrected for the parts assumed to be accommodated in the top 230 km.

thus consists of the surface left attached after the adopted moment of slab break off, corresponding to ∼300 km of convergence, as well as the surface subducted since that time. As the top 230 km of the tomographic model has not been taken into account, we need to subtract the convergence accommodated in this depth interval. For most of the Tethyan region, the lithospheric thickness in the present continental collisional setting will be on the order of 200 km. From a simple geometric point of view, the amount of convergence that needs to be subtracted from the total value will thus be 50–100 km, depending on the dip angle. When accounting for these convergence estimates, the predicted AB volumes will decrease with 15% in the Arabian region and 4% in the Indian region.

[91] While keeping the same average ages for the total lithospheric basins subducting, we reduce the maximum residence times in the mantle for the AB volumes to the adopted moments of slab break off, so t = 12 and 43 Ma. Herewith, we assume that the detached slabs sink quickly into the mantle after which the remaining slabs subduct in relatively unperturbed mantle material again. Calculations with the thermal structure of continental lithosphere instead of oceanic lithosphere could increase the AB volumes a little but will not significantly affect our results.

[92] Figure 19 shows the predicted thermal volumes (comparable for all three subduction scenarios, see caption text), corrected for the convergence assumed to be accommodated in the top 230 km. Because of the brief residence times in the mantle, the predicted thermal volumes are similar for both spreading scenarios, and do not significantly depend on the possible amount of slab thickening. The different slab break off times for the Indian region will be addressed in the comparison below.

7.2.2. Volumes Deeper in the Mantle

[93] In the Arabian region, the volumes still continuous with the deeper mantle volumes at present are assumed to include the detached slab material (Eg/SA/SI/AI of Figures 8 and 15), as well as the three Aegean and Arabian volumes (discussed above) that were probably never affected by slab break off. We will refer to these as the Arabian CD volumes hereafter. In the Indian region, the tomographic anomaly Hi (Figure 15) is selected separately as representing Spongtang lithospheric material for subduction scenario III. The CD volumes here consist of IO and IC (see Figures 8 and 15) only. The Indian break off times, that only affect the Spongtang volumes, will be discussed below. For clarity, Figure 20 only shows the predicted thermal volumes for subduction scenario III. The values for subduction scenarios I and II are comparable to these, although they lack the separate identification of a distinct Spongtang oceanic basin in the Indian region.

7.3. Comparison

7.3.1. Arabian Slab Detachment

[94] For the AB volumes in the Arabian region (Figure 19, left), the predicted thermal volumes are similar to the tomographic volumes. The cross sections through the tomographic model (Figures 4 and 5) show an interesting distribution of the anomalies along the Arabian suture zones: East of section 60, below the southern Zagros suture, the gap between the upper and lower mantle anomalies seems to be around the 660 km discontinuity. In the central area below the northern Zagros suture (sections 45–60), however, the detached lower mantle volumes have a deep ∼1000 km top. In the western Arabian region, below the Bitlis suture (i.e., west of section 35), upper mantle anomaly eT can be seen to continue in the lower mantle.

[95] The typical distribution may illustrate the lateral variation in the response on the continental collision event. The ∼660 km deep top of the eastern anomalies suggests sinking times of 13–22 Myr for free sinking rates of 3–5 cm/yr in the upper mantle. For relatively fast free sinking rates, this would be in accordance with slab break off around, or somewhat before, 12 Ma. The 1000 km deep top of the central lower mantle anomalies would correspond to sinking times of 30–40 Myr for free sinking rates of 2 cm/yr in the lower mantle. When assuming relatively fast free sinking rates again, and slab detachment ∼10 Myr after the onset of continental lithospheric subduction, a collision time around 40 Ma could explain these depths. This would be in accordance with the studies of *Dercourt et al.* [1993] and *Jolivet and Faccenna* [2000]. Lower free sinking rates would require continental collision at a much earlier

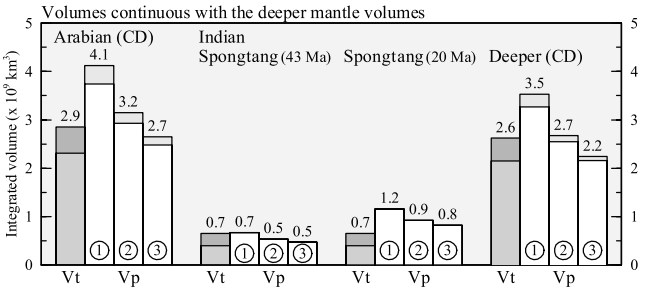

Figure 20. Tomographic volumes versus predicted thermal volumes assumed to be still continuous to the deeper mantle volumes today (CD). For clarity, the predicted volumes are given for subduction scenario III only. The Indian volumes are divided in those associated with the Spongtang remnants, for slab break off at 43 Ma and 20 Ma, and those associated with the remaining volumes.

moment, which is not supported by geological studies. We therefore propose an initiation of slab break off around ~30 Ma in the central Arabian region, below the northern Zagros suture zone, after which the tear in the slab may have propagated both eastward and westward along the suture zone. This could have led to slab break off around the expected 12 Ma underneath eastern Turkey, as well as below southern Iran.

[96] An alternative explanation of the tomographic mantle structure could be that no Cenozoic slab break off occurred, and that the tomographic anomalies of group AB represent the complete Semail oceanic lithosphere. However, the total thermal volumes predicted for the Semail slab (Figure 17, right) are much too large to be explained by these tomographic volumes alone. When assuming that the Semail oceanic basin had completely overridden the Neo-Tethys by a time later than the 80 Ma taken here, the predicted thermal volumes will decrease significantly (about 30% when using 65 Ma instead of 80 Ma) but not enough to level with the tomographic volumes.

7.3.2. Indian Slab Detachment

[97] For slab break off at 43 Ma in the Indian region, the predicted AB volumes are much larger than the tomographic volumes (Figure 19, middle). Since the continuing convergence between India and Eurasia is likely to be accommodated partly by continental lithospheric deformation and thickening in the uppermost 230 km of the mantle, the estimates made for the convergence accommodated in the top 230 km may be too simple for this region. Another explanation could be that slab break off took place much later than 43 Ma, at least along part of the trench system. Figure 19 (right) therefore also shows the predicted thermal volumes for slab detachment at 20 Ma instead, as suggested by the geological studies discussed above. With a similar ~5 Myr delay time for break off, this would require an onset of subduction of continental lithosphere around 25 Ma. In that case, the predicted volumes are still almost twice the selected tomographic volumes, but this is a difference that can be easily accounted for by shallow lithospheric deformation. Also *Replumaz et al.* [2004] concluded that half of the total India-Eurasia convergence must have been absorbed by deformation north of the convergent boundary. In addition, also the ~500 km deep top of the tomographic anomaly associated with the detached material (Hi) supports slab break off as late as 20 Ma (section 95–115 in Figure 5). With free sinking rates of 3–5 cm/yr in the upper mantle, this depth can be reached in only ~10–20 Myr. As opposed to the Arabian region, relatively slow free sinking rates (~3 cm/yr) seem most likely here.

7.3.3. Volumes Deeper in the Mantle

[98] Figure 20 displays the volumes that are assumed to be continuous with the deep mantle volumes at present for subduction scenario III. The Indian volumes are divided into the one related to the Spongtang oceanic slab, for slab break off at 43 Ma and 20 Ma, and those related to the deeper volumes CD. For the predicted CD volumes in the Indian region, slab thickening by a factor of 2 seems to be sufficient to fit the tomographic volumes. Because we can expect additional material created by oceanic spreading during convergence, however, slab thickening by a factor of 3 would be necessary to leave room for this material. In the Arabian region, slab thickening by a factor of 3 appears to be needed for the predicted CD volumes to fit the tomographic volumes in any case.

[99] We use the differential CD volumes to assess the amount of active oceanic spreading in the Neo-Tethys during its subduction, by reconstructing the original surface of the additional material subducted. Therefore we perform the same thermal calculations for predicting the present thermal volumes of the material, but in a reversed order. If Neo-Tethyan spreading has occurred over the full width of the Arabian region and during the entire 200–140 Ma time interval before ridge subduction, the reconstructed surface would require an average full spreading velocity of about 1–1.5 cm/yr. For continuous spreading within the Indian Neo-Tethys during the 200–120 Ma period before ridge subduction, the reconstructed surface would correspond to an average full spreading velocity of about 1.5–2.5 cm/yr in this region.

[100] The predicted Spongtang volumes in the Indian region (middle two comparisons of Figure 20) appear to easily fit the associated tomographic volume of anomaly Hi if slab break off occurred around 43 Ma. With slab break off as late as 20 Ma, however, the predicted volumes are somewhat too large. As the anomaly of Hi extends down to 1400 km depth, and the Spongtang oceanic basin started to subduct around 65 Ma, a fast vertical subduction in the lower mantle is required. Rates of 3 cm/yr in the upper mantle (somewhat lower than suggested by *Replumaz et al.* [2004]), and rates of 2 cm/yr in the lower mantle (also proposed by *Van der Voo et al.* [1999] and *Replumaz et al.* [2004]), seem most appropriate. These results confirm previous conclusions [*Van der Voo et al.*, 1999; *Replumaz et al.*, 2004] that India has overridden its own, overturned slab.

7.4. Conclusions

[101] When including the occurrence of slab break off after the Cenozoic continental collisions into our analysis, slab thickening by a factor of 3 appears to be necessary to explain the lower mantle tomographic volumes.

[102] For the Arabian region, our results further suggest that slab break off may have occurred first, and around 30 Ma, in the central area along the northern Zagros suture zone (~sections 45–60 of Figure 7). If this has been the case, subduction of continental lithosphere must have started around 40 Ma here. Propagation of the tear in the central slab may have led to later detachment around 12 Ma in the east, as well as in the westernmost part of the region. Fast free sinking rates of ~2 cm/yr in the lower mantle can best explain the depth of the top of the detached material. We note that we found vertical rates of ~1 cm/yr in the lower mantle for the normally subducting material in this region earlier.

[103] In the Indian region, the agreement of the tomographic volumes and predicted thermal volumes for the Spongtang Ocean of subduction scenario III is encouraging. Slab detachment at 20 Ma is found to best explain the size of the volumes still attached to the surface. If detachment has occurred at 43 Ma already, a very large amount of convergence must have been accommodated in the upper 230 km of the Earth. Also the shallow depth of the detached material below western India supports break off around 20 Ma, with free sinking rates of ~2 cm/yr in the lower

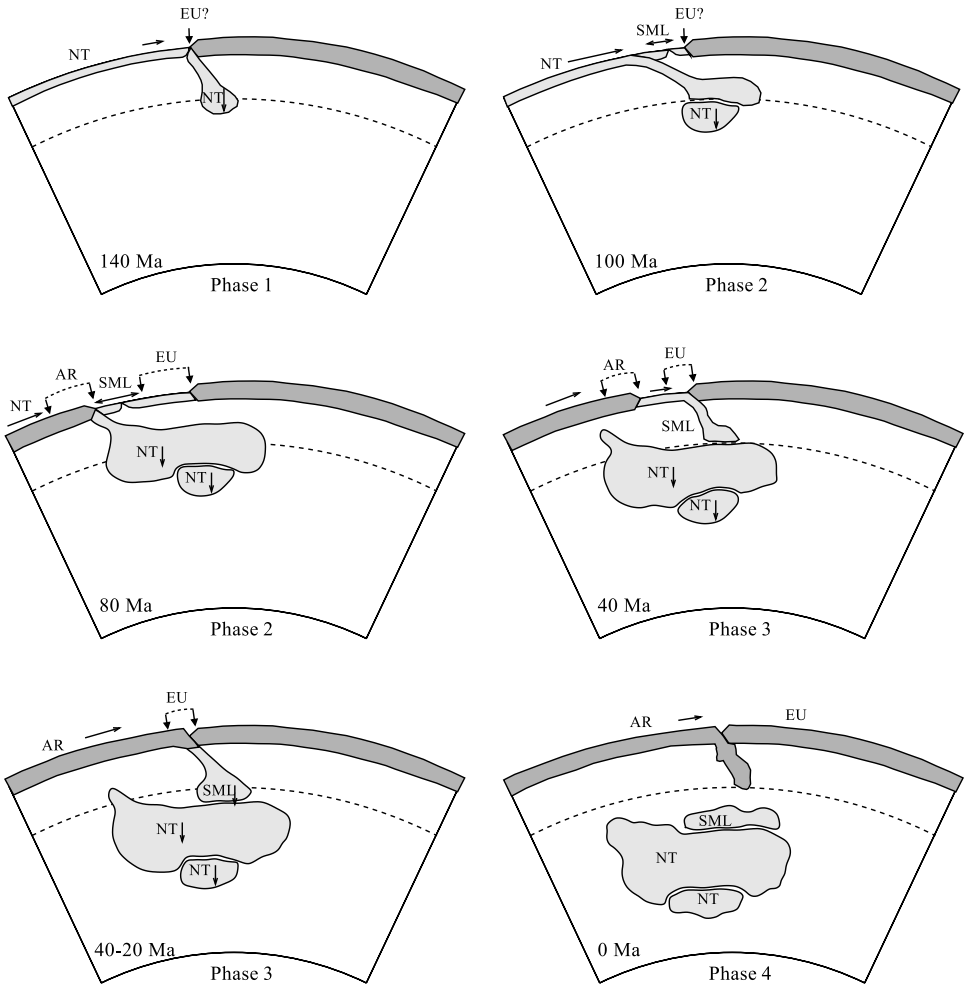

Figure 21. Reconstruction of the subduction history of the Arabian region from 140 Ma to present, for the four phases discussed in the text. The evolution is shown in an absolute reference frame, with the arrows indicating the uncertainties in the absolute positions of the continental margins (prior to 80 Ma unknown, as indicated by the question marks). The cross section for the present-day configuration is largely representative for the band of integrated tomographic anomalies shown in Figure 15 (top). Note that in Figure 15, the southernmost anomalies are the result of subduction farther south, i.e., in a section farther east, than illustrated here. EU, Eurasia; AR, Arabia; NT, Neo-Tethys; SML, Semail.

mantle as found before. An average break off time between 20 and 43 Ma, however, is found to best explain the detached volumes deeper in the mantle. Diachronous slab break off, starting at 43 Ma in the eastern Himalayas but occurring only around 20 Ma in the central and western Himalayas, would be in accordance with geological studies.

8. Reconstructing the Tethyan History of Subduction

8.1. Tethyan Subduction Model

[104] We here propose two models for the Mesozoic-Cenozoic subduction of the Tethyan oceanic lithosphere: One for the Arabian region since 140 Ma (Figure 21) and one for the Indian region since 120 Ma (Figure 22). These Tethyan subduction models obey the kinematic boundary conditions given in subduction scenario III, which was based on the plate tectonic reconstruction of *Stampfli and Borel* [2004]. Moreover, the preferred models are constructed on the basis of our interpretation of the subduction process, the analysis of the tomographic mantle structure, the absolute motion of the continental margins, and the possible effects of the Cenozoic continental collisions. The Tethyan subduction models are very similar for the Arabian and Indian regions.

[105] The cross sections shown in Figures 21 and 22 are representative for the bands of integrated tomographic anomalies in Figure 15. We emphasize that the proposed Tethyan subduction models only approximate the complicated subduction history of the Tethyan region. Evidently, the exact behavior of each slab, the timing of ridge obduction and continental collision, and the possible occurrence of slab break off all typically vary along the trench system. We note that the southernmost anomalies in the Arabian region (Figure 15, top) are the result of subduction farther south (i.e., in sections farther east) than illustrated in Figure 21, because the Arabian continental margin has not been exactly perpendicular to these sections (e.g., see Figure 8).

[106] We divide the subduction history of the Tethyan region into four phases:

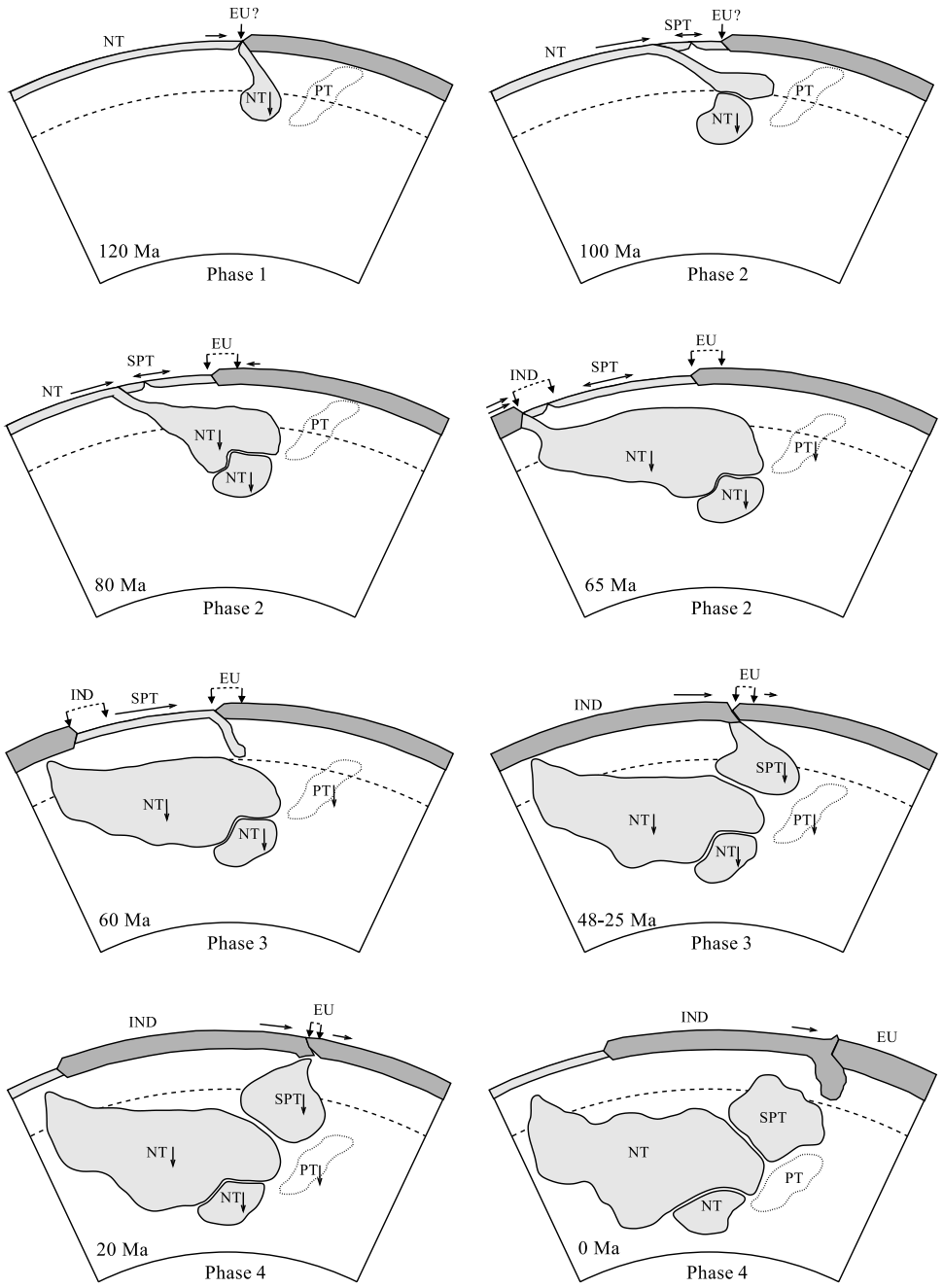

Figure 22. Reconstruction of the subduction history of the Indian region from 120 Ma to present as in Figure 21 (cf. integrated tomographic anomalies in Figure 15 (bottom)). EU, Eurasia; IND, India; PT, Paleo-Tethys; NT, Neo-Tethys; SPT, Spongtang.

[107] Phase 1 encompasses subduction of the Neo-Tethys underneath the Eurasian continental margin, followed by ridge subduction in Early Cretaceous times. The absolute positions of the continental margins, uncertain prior to 80 Ma as indicated by the question marks in Figures 21 and 22, are taken here with the Eurasian craton held fixed. The subducted part of the Neo-Tethyan lithosphere slowly sinks down into the mantle thereafter.

[108] Phase 2 comprises subduction of the remaining part of the Neo-Tethys underneath the southward extending back arcs of the Arabian Semail Ocean and Indian Spongtang Ocean, followed by collision of the back arcs onto the approaching Arabian/Indian continental margins. The relative fast trench migration causes the Neo-Tethyan slab to flatten and spread under the full width of the back-arc basins.

[109] Phase 3 starts after complete subduction of the Neo-Tethys, around 80 Ma in the Arabian region and 65 Ma in the Indian region, when the back-arc oceanic basins are being subducted underneath the Eurasian continental margin instead. As the Arabian/Indian continents move farther northward, the subducted Neo-Tethyan lithosphere is left behind within the underlying mantle. Semail/Spongtang subduction is followed by collision of the Arabian/Indian and Eurasian continents.

[110] In phase 4, subduction of Arabian continental lithosphere underneath Eurasia causes the Semail slab to break off around 12 Ma but probably around 30 Ma already in the central Arabian region. Continuous subduction of Indian continental lithosphere results in detachment of the Spongtang slab around 43 Ma in the eastern Himalayas, but only around 20 Ma in the central and western parts of the Indian region.

8.2. Requirements and Implications

8.2.1. Slab Thickening

[111] From our comparison between the predicted thermal volumes and the tomographic volumes, we can draw the important conclusion that only in the case the slab material has thickened by a factor of 3 there is space for the additionally subducted material expected to be created by oceanic spreading during convergence.

8.2.2. Free Sinking Rates

[112] The positions of the different tomographic anomalies require free sinking rates of about 3 cm/yr in the upper mantle and 2 cm/yr in the lower mantle. The fast and large-scale flattening of subducting lithosphere in the preferred model would allow for the subducted material to pile up above the 2000 km depth.

8.2.3. Locations

[113] In the Tethyan subduction model, the more recently subducted part of the Neo-Tethys ends up south of the earlier subducted part, as opposed to what one might think. Moreover, one Neo-Tethyan slab is coupled to both the northern and southern lower mantle anomalies of the tomographic model, even though these seem to be imaged as separate volumes.

8.2.4. Additional Spreading

[114] Our preferred model leaves room for the additional material expected for the probably active oceanic spreading in the Neo-Tethys during its subduction. We found that the differential volumes may correspond to average full spreading velocities of about 1–1.5 cm/yr in the Arabian region and 1.5–2.5 cm/yr in the Indian region.

8.2.5. Arabian Slab Detachment

[115] For the Arabian region, slab break off around 30 Ma in the central area, and around 12 Ma in the more western and eastern parts, can best explain the sizes and positions of the analyzed tomographic volumes. Our findings suggest an onset of subduction of continental lithosphere around 40 Ma in the central region.

8.2.6. Indian Slab Detachment

[116] Indian slab detachment around 43 Ma in the east, but merely around 20 Ma more to the west, can best explain both the depths and volumes of the tomographic anomalies underneath the Himalayas. This implies that the continuing convergence between the Indian and Eurasian continents must have been partly accommodated by the deformation of earlier accreted continental blocks and lithospheric thickening above 230 km depth.

9. Conclusions

[117] Three broadly accepted subduction scenarios for the Tethyan oceanic lithosphere and its spreading ridges, based on the plate tectonic reconstructions of *Dercourt et al.* [1993], *Şengör and Natal'in* [1996], *Norton* [1999], and *Stampfli and Borel* [2002, 2004], have been investigated by comparing the predicted thermal signature of the subducted lithosphere to the tomographic mantle structure underneath the Tethyan region. From our various analyses we draw the following conclusions:

[118] 1. The predicted thermal volumes associated with the Tethyan continent-continent convergence alone are similar for all three subduction scenarios analyzed here. The bulk volumes can well explain the tomographic volumes if most lithosphere subducted in the Tethyan region is assumed to have thickened by a factor of 2 or 3 in the mantle. This is indeed necessary in view of the large amount of Tethyan subducted lithosphere and the bulk tomographic volumes, and in agreement with laboratory and numerical studies [e.g., *Gaherty and Hager*, 1994; *Christensen*, 1996].

[119] 2. To discriminate between the different reconstructions, we have predicted the subvolumes associated with the particular oceanic basins proposed in each subduction scenario. We compared these to the separate tomographic anomalous volumes in the Tethyan region by systematically analyzing the amount, location and timing of subduction with the size, position and geometry of the tomographic anomalies. We found that the subduction model based on the reconstruction of *Stampfli and Borel* [2004], comprising the opening of large back-arc oceanic basins within the Eurasian margin, can best explain both the volumes and the positions of the anomalous volumes.

[120] 3. For our preferred Tethyan subduction model, only a threefold thickening of the slab material allows for the expected active oceanic spreading in the Neo-Tethys during its subduction. From the estimated differences between the predicted and tomographic volumes, we inferred average full spreading velocities of about 1–1.5 cm/yr in the Arabian region, and 1.5–2.5 cm/yr in the Indian region, during subduction of the Neo-Tethys.

[121] 4. Free sinking rates of about 3 cm/yr in the upper mantle and 2 cm/yr in the lower mantle seem to best explain the tomographic mantle structure in the proposed subduction model. Moreover, the model encompasses large-scale accumulation of slab material above 2000 km depth up to depths of 1000 km.

[122] 5. An Oligocene initiation of slab break off underneath the northern Zagros suture zone, and diachronous Eocene to Miocene break off below the eastern to western Himalayas, were found to best explain the volumes and depths of the associated slabs. We propose break off times of 30 Ma in the central Arabian region, and 12 Ma in its most western and eastern parts. For the Indian region, our results support 43 Ma to about 20 Ma break off times in the eastern to western Himalayas.

[123] Finally, our approach was found to enable us to successfully integrate the information contained in plate tectonic reconstructions and seismic tomographic models, and put further constraints on the subduction history of an ocean that is entirely lost today.

[124] **Acknowledgments.** We are grateful to ExxonMobil Exploration for the use of their reconstruction, for which the data were compiled by the PLATES project at the University of Texas. We very much appreciated the constructive comments of Rob van der Voo and an anonymous reviewer, as these have led to a significant improvement of our manuscript. Gérard Stampfli is thanked for his permission to include Figure 2. This work was conducted under the program of the Netherlands Research Centre

for Integrated Solid Earth Sciences (ISES) and the Vening Meinesz Research School of Geodynamics (VMSG).

References

Becker, T. W., C. Faccenna, R. J. O'Connell, and D. Giardini (1999), The development of slabs in the upper mantle: insights from numerical and laboratory experiments, *J. Geophys. Res.*, *104*, 15,207–15,226.

Bijwaard, H., and W. Spakman (2000), Nonlinear global P-wave tomography by iterated linearized inversion, *Geophys. J. Int.*, *141*, 71–82.

Bijwaard, H., W. Spakman, and E. R. Engdahl (1998), Closing the gap between regional and global travel time tomography, *J. Geophys. Res.*, *103*, 30,055–30,078.

Bunge, H.-P., and S. P. Grand (2000), Mesozoic plate-motion history below the northeast Pacific Ocean from seismic images of the subducted Farallon slab, *Nature*, *405*, 337–340.

Bunge, H.-P., M. A. Richards, C. Lithgow-Bertelloni, J. R. Baumgardner, S. P. Grand, and B. A. Romanowicz (1998), Time scales and heterogeneous structure in geodynamic Earth models, *Science*, *280*, 91–95.

Cammarano, F., S. Goes, P. Vacher, and D. Giardini (2003), Inferring upper-mantle temperatures from seismic velocities, *Phys. Earth Planet. Inter.*, *138*, 197–222.

Carminati, E., M. J. R. Wortel, W. Spakman, and R. Sabadini (1998), The role of slab detachment processes in the opening of the western-central Mediterranan basins: Some geological and geophysical evidence, *Earth Planet. Sci. Lett.*, *160*, 651–665.

Christensen, U. R. (1996), The influence of trench migration on slab penetration into the lower mantle, *Earth Planet. Sci. Lett.*, *140*, 27–39.

Chung, S.-L., C.-H. Lo, T.-Y. Lee, Y. Zhang, Y. Xie, X. Li, K.-L. Wang, and P.-L. Wang (1998), Diachronous uplift of the Tibetan plateau starting 40 Myr ago, *Nature*, *394*, 769–773.

Daniel, A. J., N. J. Kusznir, and P. Styles (2001), Thermal and dynamic modeling of deep subduction of a spreading center: Implications for the fate of the subducted Chile Rise, southern Chile, *J. Geophys. Res.*, *106*(B3), 4293, doi:10.1029/1998JB900028.

Davies, J. H., and F. von Blanckenburg (1995), Slab breakoff: A model of lithosphere detachment and its test in the magmatism and deformation of collisional orogens, *Earth Planet. Sci. Lett.*, *129*, 85–102.

Deal, M. M., G. Nolet, and R. D. van der Hilst (1999), Slab temperature and thickness from seismic tomography: 1. Method and application to Tonga, *J. Geophys. Res.*, *104*, 28,789–28,802.

De Jonge, M. R., M. J. R. Wortel, and W. Spakman (1994), Regional scale tectonic evolution and the seismic velocity structure of the lithosphere and upper mantle: The Mediterranean region, *J. Geophys. Res.*, *99*, 12,091–12,108.

Dercourt, J., L. E. Ricou, and B. Vrielynck (Eds.) (1993), *Atlas Téthys, Palaeoenvironmental Maps*, Elsevier, New York.

Duncan, R. A., and M. A. Richards (1991), Hotspots, mantle plumes, flood basalts, and true polar wander, *Rev. Geophys.*, *29*, 31–50.

Forte, A. M., R. L. Woodward, and A. M. Dziewonski (1994), Joint inversions of seismic and geodynamic data for models of three-dimensional mantle heterogeneity, *J. Geophys. Res.*, *99*, 21,857–21,877.

Gaherty, J. B., and B. H. Hager (1994), Compositional vs. thermal buoyancy and the evolution of subducted lithosphere, *Geophys. Res. Lett.*, *21*, 141–144.

Goes, S., and S. van der Lee (2002), Thermal structure of the North American uppermost mantle inferred from seismic tomography, *J. Geophys. Res.*, *107*(B5), 2050, doi:10.1029/2000JB000049.

Griffiths, R. W., R. I. Hackney, and R. D. van der Hilst (1995), A laboratory investigation of effects of trench migration on the descent of subducted slabs, *Earth Planet. Sci. Lett.*, *133*, 1–17.

Guillou-Frottier, L., J. Buttles, and P. Olson (1995), Laboratory experiments on the structure of subducted lithosphere, *Earth Planet. Sci. Lett.*, *133*, 19–34.

Hafkenscheid, E. (2004), *Subduction of the Tethys Oceans Reconstructed From Plate Kinematics and Mantle Tomography*, *Geol. Ultraiectina*, vol. 241, pp. 1–208, Utrecht Univ., Utrecht, Netherlands.

Hall, R., and W. Spakman (2002), Subducted slabs beneath the eastern Indonesia-Tonga region: Insights from tomography, *Earth Planet. Sci. Lett.*, *201*(2), 321–336.

Han, L., and M. Gurnis (1999), How valid are dynamic models of subduction and convection when plate motions are prescribed?, *Phys. Earth Planet. Inter.*, *110*, 235–246.

Jolivet, L., and C. Faccenna (2000), Mediterranean extension and the Africa-Eurasia collision, *Tectonics*, *19*(6), 1095–1106.

Kárason, H., and R. D. van der Hilst (2000), Constraints on mantle convection from seismic tomography, in *The History and Dynamics of Global Plate Motions*, *Geophys. Monogr. Ser.*, vol. 121, edited by M. A. Richards, R. G. Gordon, and R. D. van der Hilst, pp. 277–288, AGU, Washington, D. C.

Karato, S.-I. (1993), Importance of anelasticity in the interpretation of seismic tomography, *Geophys. Res. Lett.*, *20*(15), 1623–1626.

Keskin, M. (2003), Magma generation by slab steepening and breakoff beneath a subduction-accretion complex: An alternative model for collision-related volcanism in eastern Anatolia, Turkey, *Geophys. Res. Lett.*, *30*(24), 8046, doi:10.1029/2003GL018019.

Kohn, M. J., and C. D. Parkinson (2002), Petrologic case for Eocene slab breakoff during the Indo-Asian collision, *Geology*, *30*(7), 591–594.

Lay, T. (1994), The fate of descending slabs, *Annu. Rev. Earth Planet. Sci.*, *22*, 33–61.

Lithgow-Bertelloni, C., and M. A. Richards (1998), The dynamics of Cenozoic and Mesozoic plate motions, *Rev. Geophys.*, *36*, 27–78.

Mahéo, G., S. Guillot, J. Blichert-Toft, Y. Rolland, and A. Pêcher (2002), A slab breakoff model for the Neogene thermal evolution of South Karakorum and South Tibet, *Earth Planet. Sci. Lett.*, *195*(1–2), 45–58.

McClusky, S., et al. (2000), Global Positioning System constraints on plate kinematics and dynamics in the eastern Mediterranean and Caucasus, *J. Geophys. Res.*, *105*, 5695–5719.

McKenzie, D. P. (1970), Temperature and potential temperature beneath island arcs, *Tectonophysics*, *10*, 357–366.

Minear, J. W., and M. N. Toksöz (1970), Thermal regime of a downgoing slab and new global tectonics, *J. Geophys. Res.*, *75*, 1397–1419.

Müller, R. D., J.-Y. Royer, and L. A. Lawver (1993), Revised plate motions relative to the hotspots from combined Atlantic and Indian Ocean hotspot tracks, *Geology*, *21*, 275–278.

Norton, I. O. (1999), Global plate reconstruction model, technical report, ExxonMobil Explor., Houston, Tex.

Norton, I. O. (2000), Global hotspot reference frames and plate motion, in *The History and Dynamics of Global Plate Motions*, *Geophys. Monogr. Ser.*, vol. 121, edited by M. A. Richards, R. G. Gordon, and R. D. van der Hilst, pp. 339–357, AGU, Washington, D. C.

Olbertz, D., M. J. R. Wortel, and U. Hansen (1997), Trench migration and subduction zone geometry, *Geophys. Res. Lett.*, *24*, 221–224.

O'Neill, C., D. Müller, and B. Steinberger (2003), Geodynamic implications of moving Indian Ocean hotspots, *Earth Planet. Sci. Lett.*, *215*(1–2), 151–168.

Parsons, B., and J. G. Sclater (1977), An analysis of the variation of ocean floor bathymetry and heat flow with age, *J. Geophys. Res.*, *82*, 803–827.

Ranalli, G. (1996), Seismic tomography and mineral physics, in *Seismic Modelling of the Earth Structure*, edited by E. Boschi, G. Ekström, and A. Morelli, pp. 443–461, Inst. Naz. di Geofis., Rome.

Replumaz, A., H. Kárason, R. D. van der Hilst, J. Besse, and P. Tapponnier (2004), 4-D evolution of SE Asia's mantle from geological reconstructions and seismic tomography, *Earth Planet. Sci. Lett.*, *221*(1–4), 103–115.

Richards, M. A., and D. C. Engebretson (1992), Large-scale mantle convection and the history of subduction, *Nature*, *355*, 437–440.

Röhm, A. H. E., R. Snieder, S. Goes, and J. Trampert (2000), Thermal structure of continental upper mantle inferred from S-wave velocity and surface heat flow, *Earth Planet. Sci. Lett.*, *181*, 395–407.

Schmid, C., S. Goes, S. van der Lee, and D. Giardini (2002), Fate of the Cenozoic Farallon slab from a comparison of kinematic thermal modeling with tomographic images, *Earth Planet. Sci. Lett.*, *204*, 17–32.

Şengör, A. M. C., and B. A. Natal'in (1996), Paleotectonics of Asia: Fragments of a synthesis, in *The Tectonic Evolution of Asia*, edited by A. Yin and T. M. Harrison, pp. 486–640, Cambridge Univ. Press, New York.

Stampfli, G. M., and G. D. Borel (2002), A plate tectonic model for the Paleozoic and Mesozoic constrained by dynamic plate boundaries and restored synthetic oceanic isochrons, *Earth Planet. Sci. Lett.*, *196*, 17–33.

Stampfli, G. M., and G. D. Borel (2004), The TRANSMED transects in space and time: Constraints on the paleotectonic evolution of the Mediterranean domain, in *The TRANSMED Atlas: The Mediterranean Region From Crust to Mantle*, edited by W. Cavazza et al., pp. 53–80, Springer, New York.

Steinberger, B. (2000), Slabs in the lower mantle—Results of dynamic modelling compared with tomographic images and the geoid, *Phys. Earth Planet. Inter.*, *118*, 241–257.

Tarduno, J. A., and J. Gee (1995), Large scale motion between Pacific and Atlantic hotspots, *Nature*, *378*, 477–480.

Toksöz, M. N., J. W. Minear, and B. R. Julian (1971), Temperature field of a downgoing slab, *J. Geophys. Res.*, *76*, 1113–1139.

Toksöz, M. N., N. H. Sleep, and A. T. Smith (1973), Evolution of the downgoing lithosphere and the mechanics of deep focus earthquakes, *Geophys. J. R. Astron. Soc.*, *35*, 285–310.

Torsvik, T. H., R. van der Voo, and T. F. Redfield (2002), Relative hotspot motions versus true polar wander, *Earth Planet. Sci. Lett.*, *202*, 185–200.

Trampert, J., P. Vacher, and N. Vlaar (2001), Sensitivities of seismic velocities to temperature, pressure and composition in the lower mantle, *Phys. Earth Planet. Inter.*, *124*, 255–267.

van der Hilst, R. (1995), Complex morphology of subducted lithosphere in the mantle beneath the Tonga trench, *Nature*, *374*, 154–157.

van der Hilst, R. D., S. Widiyantoro, and E. R. Engdahl (1997), Evidence for deep mantle circulation from global tomography, *Nature*, *386*, 578–584.

van der Voo, R., W. Spakman, and H. Bijwaard (1999), Tethyan subducted slabs under India, *Earth Planet. Sci. Lett.*, *171*, 7–20.

Van de Zedde, D. M. A., and M. J. R. Wortel (2001), Shallow slab detachment as a transient source of heat at midlithospheric depths, *Tectonics*, *20*(6), 868–882.

Wen, L., and D. L. Anderson (1995), The fate of slabs inferred from seismic tomography and 130 million years of subduction, *Earth Planet. Sci. Lett.*, *133*, 185–198.

Wong A Ton, S. Y. M., and M. J. R. Wortel (1997), Slab detachment in continental collision zones: An analysis of controlling parameters, *Geophys. Res. Lett.*, *24*, 2095–2098.

Wortel, M. J. R., and W. Spakman (2000), Subduction and slab detachment in the Mediterranean-Carpathian region, *Science*, *290*, 1910–1917.

E. Hafkenscheid, Shell International Exploration & Production, P.O. Box 60, NL-2280 AB Rijswijk, Netherlands.

W. Spakman and M. J. R. Wortel (corresponding author), Faculty of Geosciences, Utrecht University, P.O. Box 80021, NL-3508 TA Utrecht, Netherlands. (wortel@geo.uu.nl)